Contents lists available at ScienceDirect

Redox Biology

Research Paper

Iron-loaded transferrin (Tf) is detrimental whereas iron-free Tf confers protection against brain ischemia by modifying blood Tf saturation and subsequent neuronal damage

Nuria DeGregorio-Rocasolano[a,1], Octavi Martí-Sistac[a,b,1], Jovita Ponce[a], María Castelló-Ruiz[c], Mònica Millán[d], Verónica Guirao[a], Isaac García-Yébenes[e], Juan B. Salom[c], Pedro Ramos-Cabrer[f,2], Enrique Alborch[c], Ignacio Lizasoain[e], José Castillo[f], Antoni Dávalos[d], Teresa Gasull[a,*]

[a] Cellular and Molecular Neurobiology Research Group, Fundació Institut d'Investigació en Ciències de la Salut Germans Trias i Pujol (IGTP), 08916 Badalona, Spain
[b] Universitat Autònoma de Barcelona, 08193 Bellaterra, Spain
[c] Unidad Mixta de Investigación Cerebrovascular, Instituto de Investigación Sanitaria Hospital Universitario y Politécnico La Fe-Departamento de Fisiología, Universidad de Valencia, Valencia 46026, Spain
[d] Department of Neurosciences, Hospital Universitari Germans Trias i Pujol, 08916 Badalona, Spain
[e] Departamento de Farmacología, Facultad de Medicina, Universidad Complutense de Madrid, 28040 Madrid, Spain
[f] Clinical Neurosciences Research Laboratory, Department of Neurology, Hospital Clínico Universitario, University of Santiago de Compostela, Health Research Institute of Santiago de Compostela (IDIS), 15706 Santiago de Compostela, Spain

ARTICLE INFO

ABSTRACT

Despite transferrin being the main circulating carrier of iron in body fluids, and iron overload conditions being known to worsen stroke outcome through reactive oxygen species (ROS)-induced damage, the contribution of blood transferrin saturation (TSAT) to stroke brain damage is unknown. The objective of this study was to obtain evidence on whether TSAT determines the impact of experimental ischemic stroke on brain damage and whether iron-free transferrin (apotransferrin, ATf)-induced reduction of TSAT is neuroprotective. We found that experimental ischemic stroke promoted an early extravasation of circulating iron-loaded transferrin (holo-transferrin, HTf) to the ischemic brain parenchyma. In vitro, HTf was found to boost ROS production and to be harmful to primary neuronal cultures exposed to oxygen and glucose deprivation. In stroked rats, whereas increasing TSAT with exogenous HTf was detrimental, administration of exogenous ATf and the subsequent reduction of TSAT was neuroprotective. Mechanistically, ATf did not prevent extravasation of HTf to the brain parenchyma in rats exposed to ischemic stroke. However, ATf in vitro reduced NMDA-induced neuronal uptake of HTf and also both the NMDA-mediated lipid peroxidation derived 4-HNE and the resulting neuronal death without altering Ca^{2+}-calcineurin signaling downstream the NMDA receptor. Removal of transferrin from the culture media or blockade of transferrin receptors reduced neuronal death. Together, our data establish that blood TSAT exerts a critical role in experimental stroke-induced brain damage. In addition, our findings suggest

that the protective effect of ATf at the neuronal level resides in preventing NMDA-induced HTf uptake and ROS production, which in turn reduces neuronal damage.

1. Introduction

Stroke is a life-threatening disease that causes high rates of permanent disability subsequent to neuronal loss. Neurons die as a result of interrelated processes that include glutamate excitotoxicity as a primary contributor, inflammation, and excess of free radical production. The hydroxyl radical, the most harmful of the free radicals, is generated through reactions catalyzed by iron [1,2], and several clinical and preclinical studies indicate that a previous systemic iron overload condition increases brain damage induced by ischemia [3–8].

The brain is physiologically sheltered from fluctuations of systemic iron, even under experimentally-induced systemic iron overload conditions [4,9]. However, in the ischemic brain, the detrimental effect of iron overload might result from systemic iron pools reaching the brain parenchyma. An important pool of systemic iron is known to circulate in the bloodstream bound tightly, but reversibly, to transferrin (Tf) for its transport, distribution and delivery to cells and tissues. Transferrin is present in the blood in different iron-bound forms: devoid of iron (apotransferrin, ATf), as monoferric Tf, or as diferric Tf (holo-transferrin, HTf). The relative amount of iron-free and iron-loaded Tf in blood is given in terms of the % Tf saturation (TSAT), an index that shows large differences among individuals in both diseased and healthy human cohorts [10–12]. On average, 30% of Tf in blood is saturated with iron, leaving a large amount of Tf sites available to bind iron, and leaving virtually no potentially toxic free iron in blood [13].

Cells obtain iron by receptor-mediated endocytosis of HTf through the specific interaction with the cell membrane transferrin receptor (TfR) and the classical endosome recycling pathway [14]. In brain capillaries this classical pathway co-exists with an apical-to-basolateral transcytosis of TfR ligands [15,16] through the endothelial cells from blood into the brain parenchyma [17]. Since TfR binds HTf more avidly than ATf (30-fold at physiological pH) [18,19], the circulating HTf:ATf ratio might be crucial to determine the uptake of circulating HTf through endothelial cells and into neurons, both cells types known to have membrane TfR.

To date, neither the effect of stroke on brain Tf uptake, nor the effect of TSAT on stroke-induced excitotoxic damage, nor the effect of HTf on OGD-induced neuronal reactive oxygen species (ROS) production or neuronal death have been addressed. Nonetheless, under excitotoxic conditions in vitro, it has been reported that cultured neurons or PC12 cells show an increased uptake of iron [20,21] and, noteworthy, Cheah et al. also show that glutamatergic-driven iron import by neurons is due, at least partially, to the uptake of iron bound to Tf [20].

The present study demonstrates an unreported role of transferrin and TSAT on the infarct size and neurological outcome in rat models of stroke that might have important clinical implications. This study provides the rationale, the mechanism, and the proof of concept of the beneficial effect of apotransferrin in stroke.

2. Materials and methods

2.1. Rat models of ischemic stroke by middle cerebral artery occlusion (MCAO)

Different human ischemic stroke conditions were reproduced in three models of MCAO in adult male rats: **(a)** cortical infarct through permanent MCAO (pMCAO) by ligature [22] in Sprague-Dawley rats (250–270 g, Harlan Laboratories), **(b)** cortical infarct through transient MCAO (tMCAO) (60 min) by ligature [22] in Sprague-Dawley rats (250–270 g, Harlan Laboratories), and **(c)** cortical+subcortical infarct

through tMCAO by intraluminal thread (90 min) [23] in either 1/ Sprague-Dawley rats (320–360 g, Animal Breeding Facilities of the Santiago de Compostela University, ABF-SCU) in the magnetic resonance imaging (MRI) study, or 2/ Wistar rats (300–350 g, Charles River Laboratories, [24]) for extravasation and 2,3,5-triphenyl-tetrazolium chloride (TTC)-based infarct assessment studies. Rats with a drop < 50% in laser-doppler flowmetry during the occlusion or unsuccessfully reperfused were not allocated to the experimental groups. Animals were randomly allocated to a treatment that had been concealed by a code, and the outcome was also assessed blinded. The thromboembolic stroke and reperfusion model was performed using C57 mice (around 22 g) at the European Stroke Research Platform (ESRP) by the group that first described the model [25]. Details of this model are described in that paper.

2.2. Treatments

Apotransferrin (Sigma-Aldrich) was prepared as a 50 mg/ml solution, according to the solubility data from the provider. Adult male rats weighing an average of 250 g were administered 200 mg/kg apotransferrin, 4 ml/kg i.v. in a single bolus injection (around 1 ml/rat); this is below the recommended volume of 5 ml/kg for an i.v. single bolus injection. Administration of 300 mg/kg apotransferrin or unlabelled HTf (250 mg/kg hHTf) in the High TSAT group required an i.v. slow infusion. ATf was administered at reperfusion time or 1 h after a permanent MCAO, whereas unlabelled HTf was administered before the onset of surgical procedures.

2.3. MRI

MRI was performed on a 9.4 T Bruker Biospec (Bruker Biospin) with 20 cm-wide gradients' insert of 440 mT/m. Apparent diffusion coefficient (ADC) maps were constructed by a mono-exponential pixel-by-pixel fitting of 7 echo planar diffusion-weighted images (EPI-DWI) acquired with b values of 0, 100, 300, 600, 800, 1000 and 1400 s/mm^2, echo time = 30 ms, repetition time = 4 s, and 150 μm isotropic resolution (slice thickness = 1 mm). Perfusion-weighted images (PWI) were acquired using an EPI-FAIR sequence, with echo time = 24 ms, repetition time = 10 s, 22 inversion times ranging 30–2300 ms, (selective) inversion slab = 4 mm, and 300 μm isotropic resolution (slice thickness of 2 mm).

2.4. Biochemical assessment of infarct volume

Fresh brains were cut into coronal 2 mm-thick slices and stained with 1% TTC in PBS at 37º C for 15 min. Cryopreserved paraformaldehyde-fixed mice brains were cut into 15 μm slices, collected onto poly-L-lysine-coated glass slides, and stained with cresyl violet following the procedure described by Türeyen et al. [26] with minor modifications. Infarct and hemisphere volumes were determined using ImageJ (NIH, USA) and total infarct volume was corrected for brain edema.

2.5. Neurological assessment

Each rat underwent a battery of neurological tests before pMCAO and 24 h later. We used in-lab modifications of the whiskers' stimulation response, elevated prehensile traction, corner turn, adhesive tape removal and tail-hanging response tests. The outcome of each rat in each test was assessed according to objectively measurable variables,

and a global neuroscore was assigned to each rat. The higher the score the more severe the neurological impairment. Neuroscore and infarct volume were significantly correlated (Pearson's, p = 0.0176). Neuroscore in sham-surgery rats was indistinguishable from that of undisturbed rats.

2.6. Patients

Serum samples were obtained from a cohort of 33 ischemic stroke patients that were admitted within 3 h from the onset of symptoms to the Stroke Unit of the Hospital Universitari Germans Trias i Pujol (HUGTIP). Samples were obtained at admission, before the TANDEM-1 clinical trial treatment administration (clinicalTrials.gov Identifier NCT00777140).

2.7. Determination of HTf extravasation during reperfusion in vivo

Human HTf (hHTf) (Sigma-Aldrich) was labeled with NIR fluorescent IRDye 800 (NIR-hHTf*) (LI-COR Biosciences) and administered i.v. (200 µg) at reperfusion onset. One or 2 h after reperfusion onset, rats were transcardially perfused with heparinised PBS, whole brains obtained and imaged in an Odyssey Imager System (LI-COR Biosciences), and images analyzed using ImageJ.

2.8. Western blot (WB)

Fifty µg of total protein from brain or 8 µg of total protein from cortical neurons in culture were loaded in Precast NuPAGE Midi 10% Bis-Tris (Life Technologies). MW markers (Magic Mark XP; Life Technologies) were included in 10% Bis-Tris gels, and actin or tubulin were used as tissue sample loading controls. For protein extraction addressed to detect phosphorylated proteins, we used a lysis buffer containing: 20 mM Tris-Cl pH 7.5, 137 mM NaCl, 1% Nonidet P-40, 0.5% sodium deoxycholate, 100 mM phenylmethylsulfonyl fluoride and Complete™ EDTA-free Protease Inhibitor Cocktail supplemented with 2 mM EDTA, 5 mM sodium orthovanadate and 50 mM sodium fluoride. Also, 0.26 µl of either human or rat serum, or 6 µl of cell-conditioned medium were loaded in Precast 6% TBE urea gels (U-PAGE) (Life Technologies). Human ATf (hATf) and hHTf from Sigma-Aldrich, and rat ATf (rATf) and rat HTf (rHTf) prepared in-lab from a commercial rat Tf (rTf) (Cusabio), were used as electrophoretic standards in U-PAGE. Rat ATf and rHTf were prepared following previously described protocols [27,28]. Gels were electroblotted onto PVDF-LF membranes (Millipore) which were incubated overnight at 4 °C with the specific primary antibodies and thereafter with the NIR-conjugated secondary antibodies. In WB of serum samples of rats administered with hTf, the human Tf forms (shown in red, using anti-human Tf antibody and read at 700 nm) show increased electrophoretic mobility as compared with the equivalent rat Tf forms (shown in green, using anti-rat Tf antibody and read at 800 nm). Bands were measured using an Odyssey imaging system and its dedicated software.

2.9. Calculation of TSAT (%)

The method used routinely to calculate TSAT in most reports measures iron and Tf in serum, but this method is indirect and subject to misleading results [29]. Direct assessment of transferrin saturation combining electrophoretic U-PAGE [30] (that separates Tf into ATf (devoid of iron), two monoferric Tf, and the diferric Tf bands) with band quantification has been reported to be more accurate and reliable to determine TSAT [29,31,32].

In rats receiving hTf, % TSAT arises from the mixture of all iron-free and iron-loaded forms of both the endogenous rTf and the exogenous hTf. Antibodies used were selected to avoid cross-reactivity between species and to equally recognize ATf and iron-containing Tf forms in WB.

We calculated % TSAT in serum samples of stroke patients or rats using our U-PAGE/WB results, according to the formula previously used by different groups [31,33]:

$$TSAT(\%) = (\tfrac{1}{2} \cdot mFe \cdot Tf + diFe \cdot Tf) \cdot 100 / (ATf + mFe \cdot Tf + diFe \cdot Tf)$$

2.10. Primary culture of cortical neurons

Cell cultures of rat cortical neurons were prepared as previously described [34] from male and female E18 fetuses from pregnant Sprague-Dawley rats (Envigo/Harlan). Neuronal cultures were grown in Neurobasal™ medium supplemented with 2% B-27 (Life Technologies) in oxygen and glucose deprivation (OGD) experiments or with 2% NS21 in NMDA-experiments (NS21 supplement was made in-lab to control the amount of Tf and the TSAT in the culture medium, according to ref. [35]. All experiments were performed at 12 DIV. Ninety seven % of cells in cultures were neurons. Independent experiments were performed using neurons obtained from fetuses from different pregnant rats and done on different days. Each experimental condition was tested in at least 3 independent experiments or biological replicates, each with 3–4 technical replicates (culture plate wells).

2.11. Determination of total intracellular ROS, Fe^{2+} and 4-hydroxynonenal (4-HNE)

OGD-exposed neurons were reperfused for 30 min in the presence or the absence of either HTf or $FeCl_3$ in medium containing 5-chloromethyl-2,7-dichlorodihydrofluorescein diacetate (CM-H_2DCFDA (Invitrogen, Barcelona, Spain) (10 µM), washed to remove excess dye, and fluorescence was measured. DCFH-DA easily crosses the membrane of cells in culture. Once in the cytosol, DCFH-DA is cleaved and becomes membrane-impermeable and, when oxidized, it turns into a DCF fluorophore whose emission brightness has been considered to measure the levels of cellular ROS. In some conditions, this might not measure ROS only, but rather detect radicals to which peroxides are converted by transition metal ions [36]. Therefore, DCFH-DA indeed seems especially suited to study the effect of iron released from iron-loaded transferrin on ROS formation during OGD or NMDA-induced excitotoxicity in our study. Fe^{2+} was assessed with the turn-on FeRhoNox™−1 fluorescent probe as described by Hirayama et al. [37] and obtained from Goryo Chemical Inc. (Goryo, Japan). Five µM FeRhoNox™−1 was added to the neuronal medium, incubated for 30 min in the presence of the treatments and imaged as specified by the manufacturer. 4-HNE was determined by immunocytochemistry in neurons exposed to treatments for 40 min. Images were taken using a fluorescence AxioObserver Z1 microscope (Carl Zeiss, Germany).

2.12. Neuronal viability assessment

Cell death was determined measuring the incorporation of propidium iodide (PI). We used a Varioskan flash reader (ThermoFisher Scientific, Finland) and followed the method by Rudolph and col [38] adapted in our lab [39].

2.13. OGD

The conditioned medium of 12-DIV neuron cultures was removed and saved. Neurons exposed to OGD were incubated in glucose-free DMEM in a 0.2% O_2 atmosphere in a Galaxy R+ hypoxia incubator (RSBiotech). Control cells were incubated in DMEM supplemented with 4.5 g/L glucose at normoxia. After a 90-min period incubation, cultures were returned to their conditioned medium and further incubated in normoxic conditions.

2.14. Immunocytochemistry

Neurons grown on poly-L-lysine-coated glass coverslips were fixed at 4 °C in 4% paraformaldehyde in PBS-2% sucrose, permeabilized in 100% methanol, blocked, and incubated overnight at 4 °C with the primary antibodies. Subsequently, the cultures were washed, incubated with secondary antibodies and mounted with Fluoromount (Sigma-Aldrich) or ProLong® Gold (Life Technologies). Images were generated on an AxioObserver Z1 microscope (Carl Zeiss), and obtained using an immersion oil 40x lens (N.A 1.3), a MCR5 camera and Zen Blue software (Carl Zeiss). For each treatment, 45 fields were analyzed (5 fields/well, 3 wells/treatment, 3 experiments). Quantification was performed by two researchers blind to the treatments.

To address the cellular localization of hTf, plasma membrane was stained with wheat germ agglutinin (WGA) Alexa Fluor® 488 conjugate (Life Technologies). Neurons were imaged on a confocal microscope (LSM710; Carl-Zeiss), using an immersion oil 63x lens (N.A. 1.4), a MCR5 camera and Zen Black software (Carl Zeiss).
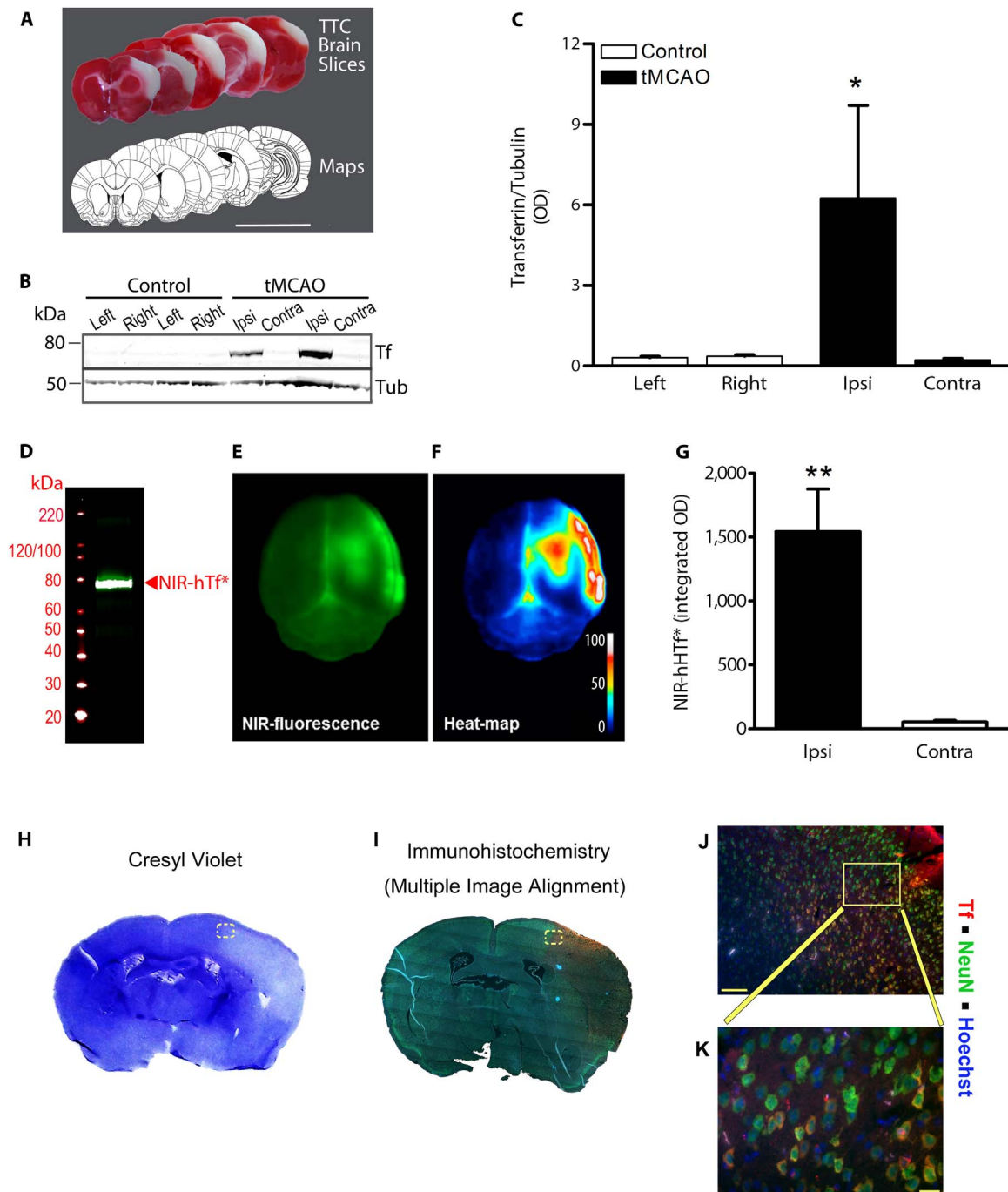

Fig. 1. Experimental stroke increases HTf extravasation into ischemic tissue and HTf increases OGD-induced neuronal death. **(A)** Representative TTC-stained brain slices of a rat exposed to tMCAO (ligature) plus 24 h reperfusion; scale bar, 1 cm. **(B)** Representative WB showing Tf and tubulin bands in the ischemic area (Ipsi) at 2 h postreperfusion and in a mirror area in the contralateral cortex (Contra) or in Control rats (Left and Right). **(C)** Transferrin/Tubulin ratio from WB bands as in (B) (n = 4 per group; paired *t*-test: *p = 0.0451). **(D)** WB NIR-hHTf*. Representative **(E)** raw fluorescence and **(F)** heat-map images of the brain of a rat exposed to tMCAO, injected i.v. with NIR-hHTf* and allowed to reperfuse for 2 h. **(G)** Quantification of the NIR-hHTf* fluorescence in the hemispheres after tMCAO/2 h reperfusion (n = 6; paired *t*-test: **p = 0.0072). Representative histological mouse brain slice images obtained using **(H)** cresyl violet or **(I)** immunohistofluorescence for NeuN (green), Tf (red) and nuclei (blue). Brains were obtained from mice exposed to thromboembolic stroke plus 24 h reperfusion. **(J-K)** show magnified images; scale bars, 100 μm (in **J**) and 20 μm (in **K**).

2.15. Immunohistochemistry

Fifteen μm slices from cryopreserved optimal cutting temperature (OCT)-embedded paraformaldehyde-fixed mice brains were obtained and collected onto poly-L-lysine-coated glass slides, exposed to antigen retrieval (95-99° C in 0.01 mol/L citrate buffer, pH 6.0, for 20 min), and incubated overnight with the primary antibodies at 4 °C and then with secondary antibodies and mounted with Fluoromount (Sigma-Aldrich F4680). Images were obtained using a fluorescence AxioObserver Z1 microscope (Carl Zeiss, Germany).

2.16. Determination of serum Tf levels

Tf levels in the serum of stroke patients and rats were determined by ELISA (Abnova; Abcam).

2.17. Neuronal uptake of hHTf in three conditions: in the presence of hATf, after specific blockade of TfR, and/or after Tf depletion from the conditioned medium (CM)

Neuronal uptake of hHTf was tracked by incubation with hHTf labeled with fluorophore Dyomics 547 (60 nM) (hHTf*; Exbio). We used hATf at concentrations suitable to compete with hHTf for their common receptor at the neuronal membrane. An anti-rat TfR monoclonal antibody (OX26, 13–26 μg/ml) was used to block the TfR. To deplete Tf from CM, two sequential immunoprecipitations were performed using the Dynabeads kit (Invitrogen) and a 1:1 mixture of two monoclonal antibodies against human Tf (HTF-14 and OT1 clones, Acris Antibodies).

Cultures were incubated in CM containing either hATf, OX26, and/or in CM depleted of Tf, before the addition of 50 μM NMDA. Fifteen min later the cultures were fixed and processed for immunocytochemistry to assess hHTf* uptake.

2.18. Antibodies

The following primary antibodies were used for immunocytochemistry or WB: rabbit anti-rat Tf polyclonal antibody (4 μg/ml, Cappel 55720), mouse anti-hTf monoclonal antibodies OT-1 and HTF-14 (5 μg/ml, Acris Antibodies BM2704 and BM745S, respectively), mouse anti-tubulin (0.25 μg/ml, Sigma-Aldrich T6074), rabbit anti-actin (0.25 μg/ml, Sigma-Aldrich A2066), rabbit anti-4-hydroxynonenal (4-HNE) (1:750, Enzo Life Sciences ALX-210–767-R100), goat anti-NRAMP 2, also known as divalent metal transporter 1 (DMT-1) (1:50, Santa Cruz Biotechnology SC-16887), rabbit anti-death-associated protein kinase 1 (DAPK1) polyclonal antibody (2 μg/ml, Sigma-Aldrich D1319), mouse anti-phospho DAPK1 (pSer308) monoclonal antibody DPKS308 (20 μg/ml, Sigma-Aldrich D4941). For immunohistochemistry, goat anti-mouse Tf polyclonal antibody (20 μg/ml, Novus Biologicals NB110-82403), rabbit anti-mouse NeuN monoclonal 27-4 antibody (1:100, Millipore MABN140) and mouse anti-rat TfR monoclonal antibody OX-26 (4 μg/ml, Santa Cruz Biotechnology SC-53059) were used. To block TfR we used the OX26 antibody. The secondary antibodies IRDye-680 donkey anti-mouse (926–68072) and IRDye-800 donkey anti-rabbit (926–32213) (1:15,000, LI-COR Bioscience) were used.

2.19. Statistics

Results are expressed as the mean ± SEM. Statistical analyses were performed using GraphPad Prism. Data were analyzed using unpaired or paired Student's t-test, or one-way ANOVA for independent or repeated measures followed by the post-hoc Student-Newman-Keuls multiple comparisons test (SNK), or Mann-Whitney U test, as required. When necessary, data were log-transformed to achieve homogeneity of variances. Pearson's correlation was used when required. The effects were considered statistically significant at $p < 0.05$.

2.20. Study approval

All the experimental protocols involving rats were approved by the Institutional Animal Care and Animal Experimentation Committees of the Centers involved, in compliance with EU directives 86/609/CEE and 2003/65/CE and conducted in conformity with international guidelines (Guide for the Care and Use of Laboratory Animals, National Institutes of Health publication 85-23, 1985), laws and policies. The TANDEM-1 clinical trial (clinicalTrials.gov Identifier NCT00777140) had the approval of the Ethical Committee of Clinical Research (CEIC) of the HUGTIP and the informed consent of all patients.

3. Results

3.1. HTf extravasates and accumulates in neurons of postischemic brain areas in experimental stroke models

In a model of tMCAO by ligature that reproducibly damages the same cortical areas 24 h after the ischemia (Fig. 1A), the Tf signal was 27-fold higher in the ipsilateral postischemic than in the contralateral area, measured 2 h after reperfusion onset (Fig. 1B-C).

To determine whether this Tf increase in the brain resulted from extravasation or from local Tf expression, near-infrared (NIR)-labeled hHTf (NIR-hHTf*) (Fig. 1D) was injected i.v. in the rat at reperfusion onset in an intraluminal tMCAO stroke model; this model avoids unspecific NIR signal interference in the brain due to blood leakage at the site of surgery (neck). Two hours after reperfusion onset, we observed a 30-fold increase in the NIR-hHTf* signal in the ipsilateral vs the contralateral brain hemisphere (Fig. 1E–G).

In addition, we found increased Tf immunostaining in neurons of the postischemic brain areas 24 h after the MCAO onset in a mouse model of thromboembolic stroke and reperfusion. Tf signal was increased in the areas identified as infarct or peri-infarct using cresyl violet staining; Tf and NeuN colocalized in the same cells, indicating accumulation of Tf in neuronal bodies (Fig. 1H–K).

3.2. HTf is harmful to neurons exposed to an in vitro model of ischemia

Using an in vitro model of ischemia by OGD, we observed that neither OGD (90-min plus 30-min reoxygenation) nor hHTf in control normoxic conditions induced early neuronal death (Fig. 2A). However, OGD did induce early neuronal death in the presence of hHTf (Fig. 2A). Importantly, we show that 5 μM exogenous hHTf increased the OGD-induced DCF emission, which is considered an index of ROS production, in neurons, whereas 50 μM free iron added to the media did not (Fig. 2B).

To our knowledge, reports showing toxicity of iron on neurons in culture have seldom, if ever, considered that Tf, an essential ingredient of most culture media, might eventually become HTf in the presence of iron. We found that free iron added to the medium incorporated into Tf present in the B27-supplemented-medium and increased the intensity of the band corresponding to diferric Tf (diFe-Tf) (Fig. 2C). Moreover, Fe^{3+}, that incorporated more efficiently than Fe^{2+} into medium Tf (see arrows in Fig. 2C), induced early cell death in OGD-exposed neurons at a lower concentration (20 μM Fe^{3+}) than Fe^{2+} (Fig. 2D). In addition, HTf induced cell death at a much lower concentration than free iron (Figs. 2A and 2D).

OGD did not increase the neuronal levels of TfR (Fig. 2E) but doubled DMT-1 levels (Fig. 2F).
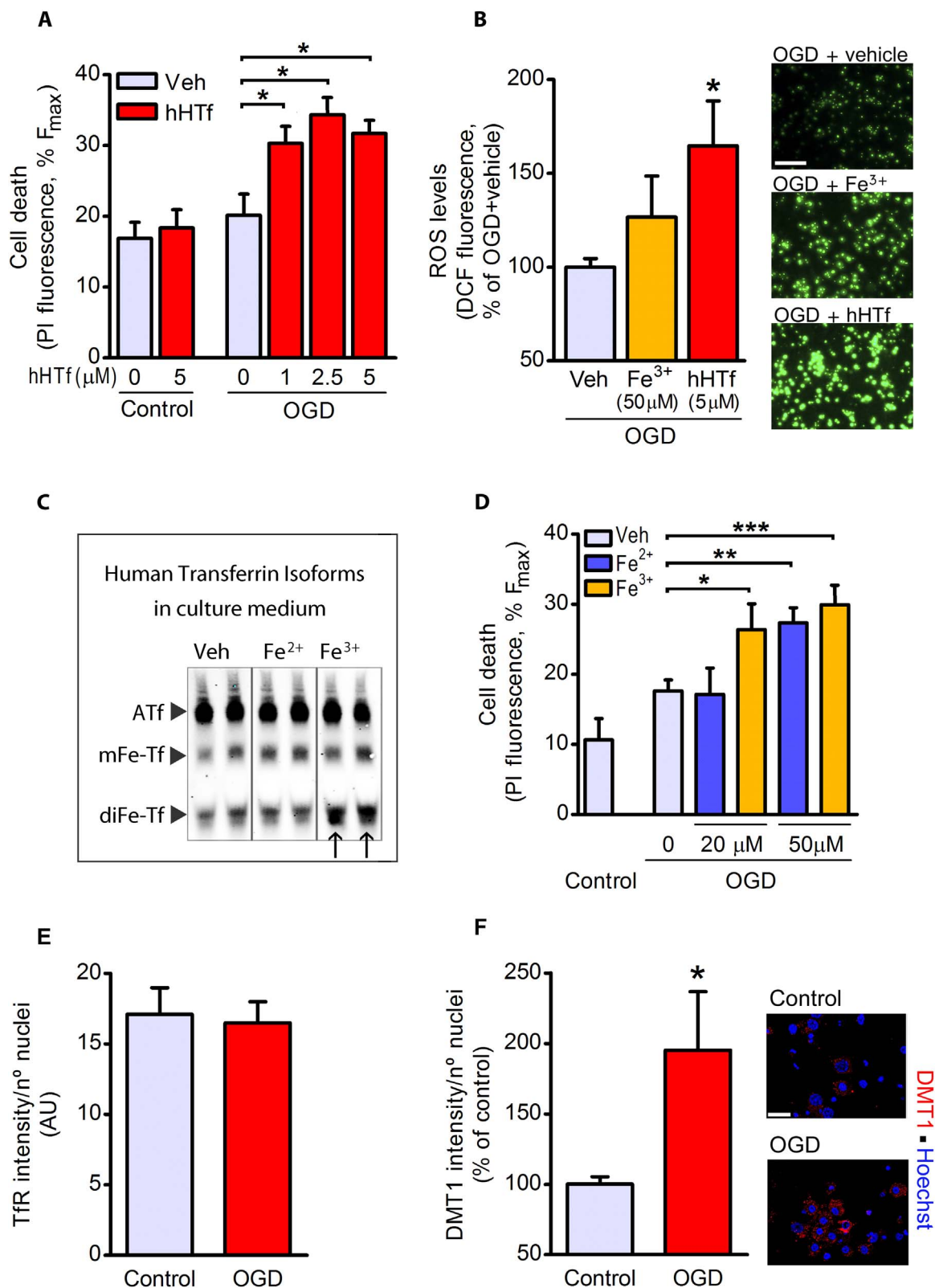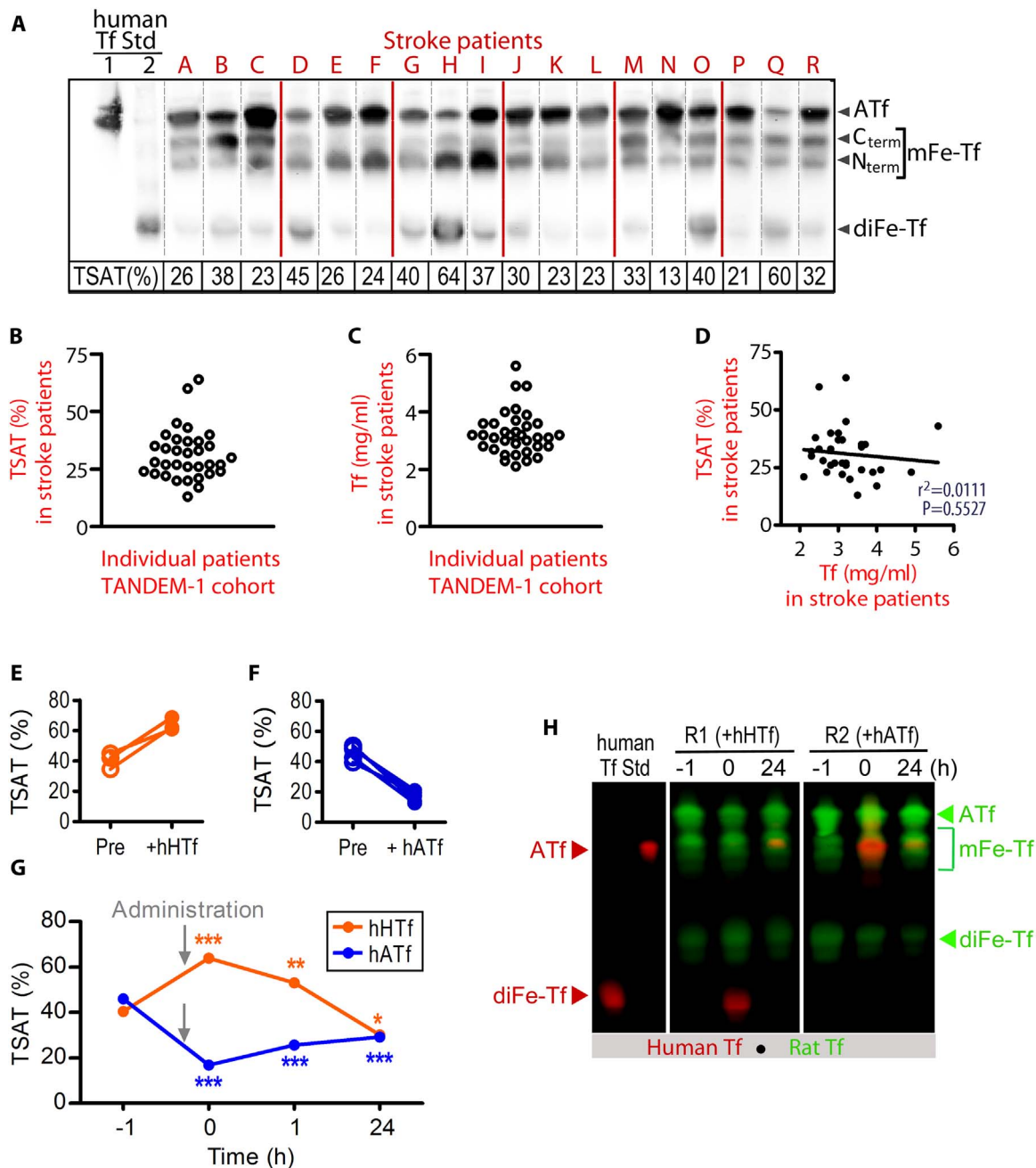
Fig. 2. HTf increases OGD-induced ROS production and neuronal death. Neuronal cultures were incubated in OGD or control conditions, while their original conditioned medium was kept in twin cell-free plates with hHTf, Fe^{2+} or Fe^{3+}. **(A)** After OGD, neurons were returned to normoxia in their own original medium, now containing hHTf, and the effect of hHTf in neuronal death was measured 30 min later (4 independent experiments, ≥ 3 wells/group/experiment; one-way ANOVA: p = 0.0014, and SNK test: *p < 0.05). **(B)** Representative images and quantification of free radical production induced by iron or HTf added during reperfusion to neurons previously exposed to OGD (3 independent experiments, ≥ 3 wells/group/experiment; one-way ANOVA: p < 0.05, and SNK test: *p < 0.05 vs neurons exposed to OGD without additional treatment). Scale bar; 100 μm. **(C)** Representative U-PAGE/WB showing the bands of ATf, mFe-Tf and diFe-Tf as present in the cell-free culture medium incubated with vehicle, 20 μM Fe^{2+} or 20 μM Fe^{3+} for 90 min. Transferrin present in the media was that included by the commercial supplier in the standard formulation of B-27-supplemented medium. **(D)** Effect of Fe^{2+} and Fe^{3+} on neuronal death in OGD-exposed cultures as measured 30 min after the onset of reoxygenation (3 independent experiments, ≥ 3 wells/group/experiment; one-way ANOVA: p = 0.0027 for Fe^{2+} and p = 0.0002 for Fe^{3+}, and SNK test: *p < 0.05, **p < 0.01, ***p < 0.001). **(E-F)** Effect of 90 min OGD on the levels of **(E)** TfR and **(F)** DMT-1 as assessed by immunocytochemistry (3 independent experiments, ≥ 3 wells/group/experiment; Mann-Whitney *U* test: *p = 0.028).

3.3. Top and bottom TSAT values observed in serum from stroke patients can be reproduced in the rat by the administration of HTf or ATf, respectively

We first determined TSAT in the serum collected from stroke patients at admission, by a direct method using U-PAGE/WB that separates bands, each band corresponding to different human transferrins with regard to their iron cargo (Fig. 3A). Mean TSAT values in stroke patients samples was $31.2 \pm 1.9\%$, showing large individual differences with values ranging from 13% to 64% (Fig. 3A–B); serum Tf

concentration did not correlate with TSAT ($r^2 = 0.011$, $p = 0.553$) (Fig. 3C–D).

Next, to reproduce the top and bottom blood TSAT observed in these patients, rats received, respectively, hHTf or hATf i.v., and the new TSAT was calculated (Fig. 3E-F). Baseline TSAT was $44.0 \pm 1.9\%$ in undisturbed rats (Fig. 3G), similarly to sham-operated rats (not shown), and higher than the average TSAT in stroke patients. Administration of 250 mg/Kg hHTf i.v. to rats increased TSAT to $63.9 \pm 2.4\%$ within minutes and remained increased 1, but not 24, h later. Conversely, i.v. administration of 300 mg/Kg hATf decreased TSAT to $16.9 \pm 1.6\%$

Fig. 3. Top and bottom blood TSAT measured in stroke patients are reproduced in rats administered HTf or ATf, respectively. **(A)** U-PAGE/WB showing the electrophoretic pattern of hATf, C-term and N-term monoferric Tf (mFe-Tf) forms, and diferric Tf (diFe-Tf) form in representative serum samples of stroke patients (red lines separate different gels). Human ATf and hHTf standards were loaded in lanes 1 and 2, respectively. TSAT calculated individually for each patient is indicated below each lane. **(B)** Individual TSAT values and **(C)** individual Tf serum levels of 33 stroke patients, obtained at admission, **(D)** do not correlate. **(E-F)** Effect of the administration of **(E)** hHTf or **(F)** hATf on TSAT in each individual rat. **(G)** Time-course of TSAT before and after the administration of hHTf or hATf (n = 3–5 per group; repeated measures one-way ANOVA: p = 0.0186 for hHTf and p < 0.0001 for hATf administration, and SNK test: *p < 0.05, **p < 0.01, ***p < 0.001 vs before administration (t = − 1). **(H)** Representative U-PAGE/WB showing human (red) and rat (green) bands of ATf, mFe-Tf and diFe-Tf in rat blood before (t = − 1) and after (t = 0 and 24 h) administration of exogenous hHTf or hATf. The human Tf forms have increased electrophoretic mobility as compared with the equivalent rat Tf forms (e.g. note that human ATf and rat monoferric transferrin show similar electrophoretic mobility).

within minutes, and remained significantly below pre-administration levels 1 and 24 h later (Fig. 3G).

Iron isoforms of rat and human Tf have different electrophoretic mobility (Fig. 3H). Levels of exogenous Tf, administered either as hATf or hHTf, remained steady in blood during the first hour post-administration. Exogenous hATf not cleared from rat circulation after a 24-h period mainly remained in its iron-free form (Figs. 3H and 7A), whereas exogenous hHTf lost all its iron and converted to hATf after a 24-h period (Fig. 3H).

3.4. High TSAT increases infarct volume and mortality in rats exposed to tMCAO

Using the set up conditions shown in experiments in Fig. 3, we next increased rats' TSAT up to 64% (High TSAT group, which mimics top TSAT values in stroke patients) by the administration of hHTf (250 mg/Kg) or maintained baseline TSAT before they received intraluminal tMCAO (90 min). A magnetic resonance imaging (MRI) study was carried out to get the time-course evolution of hypoperfused or infarcted areas in the brain. TSAT still remained increased at the end of the MRI acquisition period (3 h). No differences were found in the volume of brain tissue showing hypoperfusion in MRI perfusion-weighted imaging (PWI) between vehicle and hHTf-treated rats (approximately 270 mm^3 of brain showed hypoperfusion during the occlusion period, Fig. 4A). Higher diffusion-weighted imaging (DWI) volume was found in hHTf-treated rats when compared with vehicle-treated rats, starting 35 min after the occlusion (Fig. 4B–C). Brain tissue with reduced blood perfusion (PWI volume) but not included in the lesion core (DWI volume) indicates penumbral potentially salvageable tissue, according to the PWI-DWI mismatch concept [40]. We found that, 70 min after reperfusion onset, vehicle- and hHTf-treated tMCAO rats had 188.0 ± 46.3 mm^3 and 33.3 ± 35.3 mm^3 of salvageable tissue, respectively (Fig. 4D). This indicates that High TSAT rats have almost no salvageable tissue assessed 70 min after reperfusion (160 min post MCAO), whereas approximately 70% of the brain volume at risk is still salvageable in the animals in the vehicle group. Moreover, mortality during the first 24 h following tMCAO in the High TSAT group was 50% whereas in the vehicle group was 23%, being the later the mortality usually associated to this stroke model.

3.5. Lowering TSAT at reperfusion reduces infarct volume in rats exposed to tMCAO

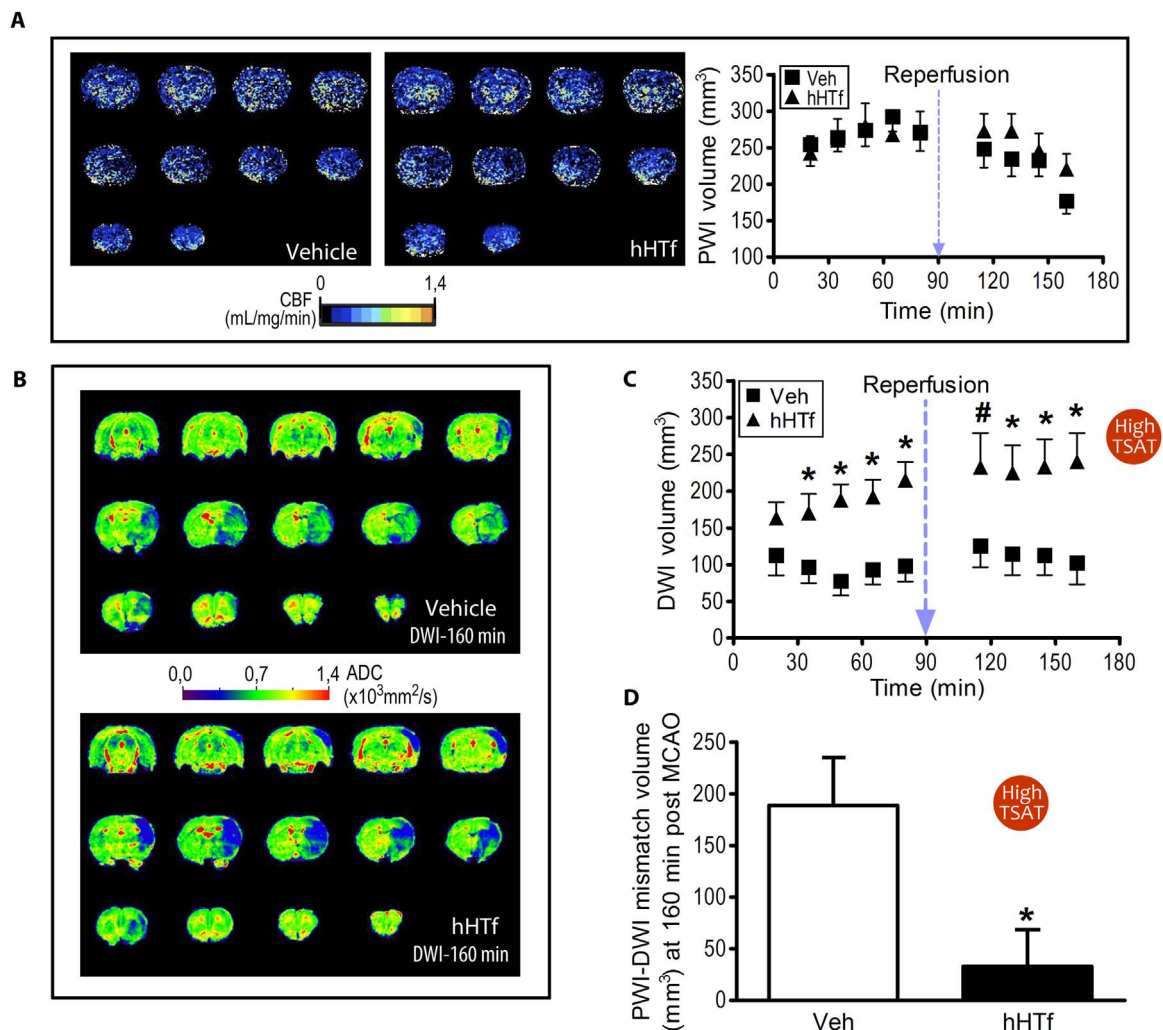Since intraluminal tMCAO rats with normal baseline TSAT levels

Fig. 4. Experimentally-induced High TSAT with hHTf increases brain damage volume in rats exposed to tMCAO. **(A)** Representative MRI-PWI coronal sections of rat brains 70 min after ischemia onset (tMCAO by intraluminal thread) in Veh-treated (left) and hHTf-treated rats (middle). Time-course effect of hHTf-High TSAT on hypoperfused-PWI brain volume during ischemia and early reperfusion (right) (n = 8–12 per group). **(B)** Representative ADC maps obtained from DWI of coronal rat brain sections of tMCAO rats (Vehicle, top; hHTf-treated, bottom) 160 min after the ischemia onset. **(C)** Time-course effect of hHTf-High TSAT on lesion-DWI volumes during ischemia and early reperfusion (n = 8–12 per group; t-test: *p < 0.05, #p = 0.0563 vs respective Veh). **(D)** Salvageable hypoperfused brain tissue as assessed by PWI-DWI mismatch 160 min after the ischemia onset in normal TSAT (Veh) and High TSAT (hHTf) rats (n = 8–12 per group; t-test: *p = 0.0216).

still have a large area of salvageable brain tissue at postreperfusion (Fig. 4D), we next reduced TSAT to 17% by hATf administration at reperfusion in the Low TSAT-17 group and found a 50% reduction in the infarct volume 24 h later (Fig. 5A). The protection was larger in the cortex than in the subcortical area (Fig. 5B).

We then reduced TSAT to 25% (Low TSAT-25) at reperfusion in a model of tMCAO by ligature, known to affect specifically cortical areas only, and obtained a larger protective effect 24 h later (Fig. 5C–D).

3.6. Lowering TSAT reduces brain damage and ameliorates neurological outcome in an experimental model of pMCAO

Since High TSAT-induced damage begins before reperfusion onset (DWI-MRI data above), we hypothesized that reduction of TSAT might be therapeutic without recanalization. To test this, we reduced TSAT (Fig. 6A–B) (Low TSAT) 1 h after the onset of pMCAO by ligature, and found a 60% reduction of the infarct volume (Fig. 6C–D) and also of the neurological deficit (neuroscore) 24 h later (Fig. 6E). Also, TSAT measured right after hATf administration showed a positive correlation with the infarct volume (Fig. 6F) and also the neuroscore (Fig. 6G), as assessed at 24 h. Moreover, ATf therapy reduced pMCAO-induced body weight loss (Fig. 6H).

3.7. ATf treatment does not block the MCAO-induced extravasation of HTf

Human ATf given to pMCAO rats 1 h following the occlusion and not cleared from circulation remains in blood as hATf 24 h later (Fig. 7A), indicating that protection by hATf is unrelated to its iron-

binding capacity in blood. To determine whether hATf therapy might block the TfR-mediated HTf transport through the blood brain barrier (BBB) during stroke, rats received vehicle or hATf i.v. (300 mg/Kg) at reperfusion onset together with exogenous NIR-labeled hHTF (NIR-hHTf*, < 0.4% of the endogenous blood Tf levels). Exogenous NIR-hHTf* was determined in brain hemispheres while still largely saturated in blood, 1 h after administration (Fig. 7B). One hour after reperfusion, NIR-hHTf* signal was > 50% higher in the ipsilateral-ischemic brain hemisphere than in the contralateral one, regardless rats had been treated or not with hATf (Fig. 7C). Therefore, ATf does not prevent MCAO-induced NIR-hHTf* uptake in the postischemic brain hemisphere. Also, the ipsilateral brain hemisphere accumulated 3.7-fold more exogenous hATf than the contralateral hemisphere 1 h postreperfusion (Fig. 7D–E).

3.8. Protection by a direct action of ATf at the neuronal level: ATf prevents NMDA-mediated HTf uptake by neurons and subsequent neuronal death

As expected, blockade of NMDA receptors (NMDAR) with MK-801 fully protected against OGD-induced neuronal death (Fig. 8A). Also, NMDA in vitro drives import of iron into neurons which is due, at least partially, to uptake of Tf-bound iron pool (ref. [20] and Figs. 8B and 9B). Within this framework, and since protection by ATf is not due to a blockade in the extravasation of Tf, we next studied whether ATf competes with HTf at the neuronal level. Human ATf (≥ 12 μM) prevented the NMDA-induced increase in neuronal uptake of hHTf* (Fig. 8B–C); most hHTf* incorporated was located in the cytoplasm (Fig. 8C). In neurons exposed to NMDA, addition of 0.1 μM hHTf to the
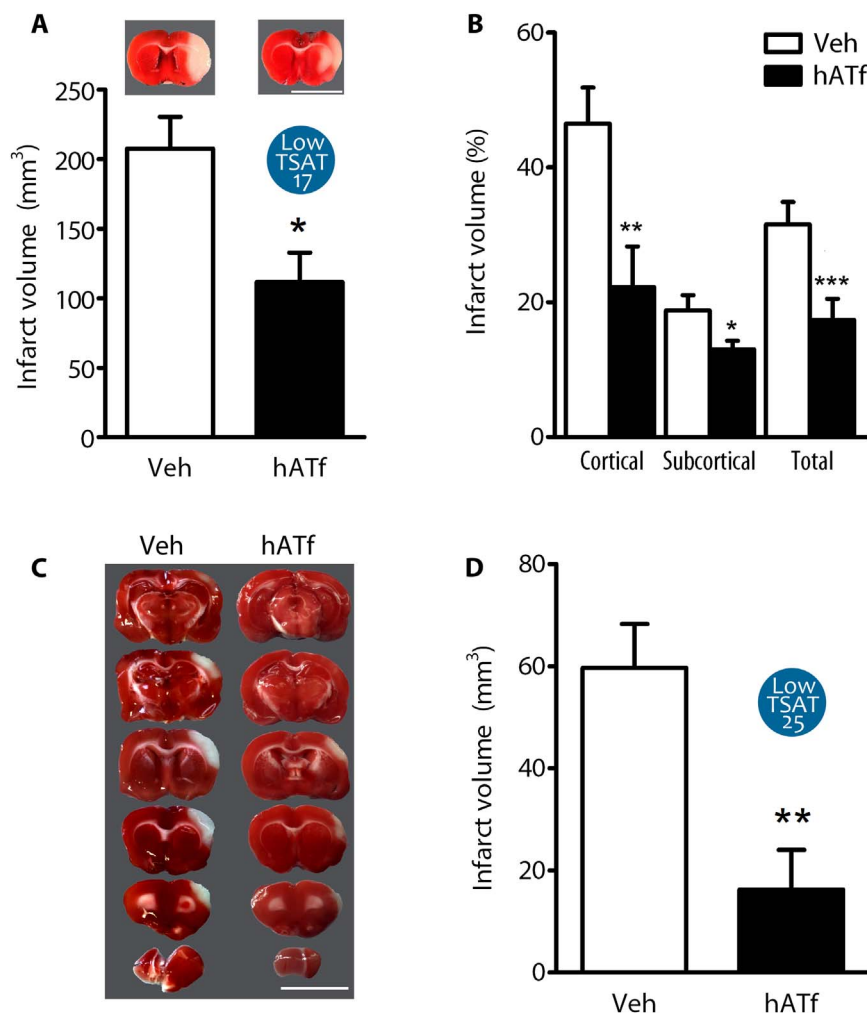

Fig. 5. Experimentally-induced Low TSAT at reperfusion reduces the infarct volume in tMCAO rats. (A) Effect of reduction of TSAT to 17% (Low TSAT-17) by the administration of 300 mg/Kg hATf i.v. at reperfusion on the infarct volume (TTC staining) of tMCAO rats (intraluminal filament model); scale bar, 1 cm (n = 6–7 per group; t-test: *p = 0.0103). Representative TTC-stained brain slices are shown on top of each bar. (B) Effect of Low TSAT-17 on % infarct volume in cortical and subcortical brain regions (n = 6–7 per group; t-test: *p = 0.0436, **p = 0.0133, ***p = 0.0102 vs respective Veh). (C) Representative TTC-stained brain sections of rats treated at reperfusion with Veh or 200 mg/Kg hATf (Low TSAT-25), 24 h after tMCAO (ligature model); this model infarcts only cortical areas; scale bar, 1 cm. (D) Quantification of the effect of treatment with 200 mg/Kg hATf in the tMCAO model indicated in (C) (n = 6–7 per group; t-test: **p = 0.0036).
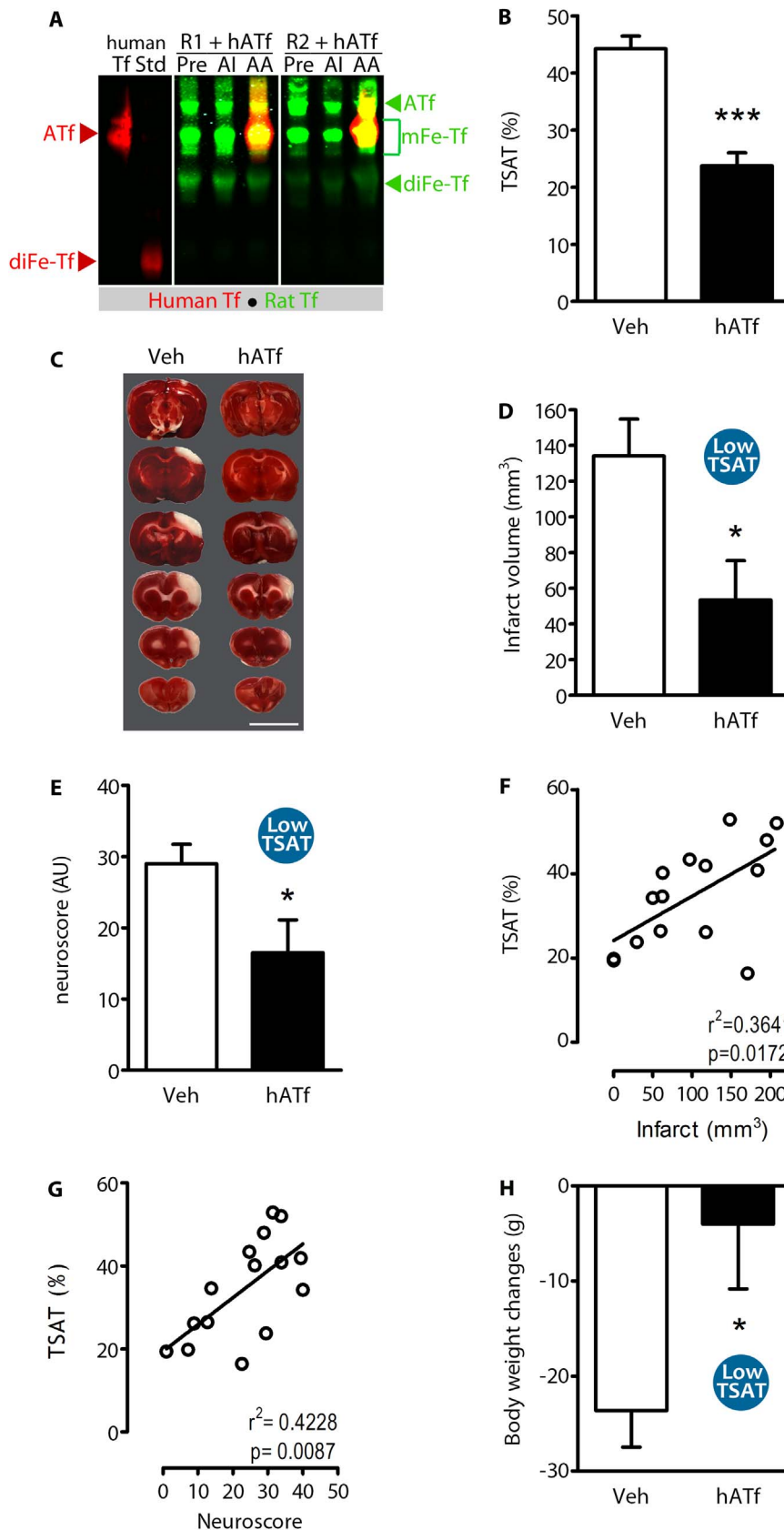
Fig. 6. TSAT reduction diminishes brain damage and improves neurological performance in experimental permanent stroke. **(A)** Representative U-PAGE/WB showing the ATf, mFe-Tf, and the diFe-Tf bands of rat Tf (green) and iron forms of human Tf (red) in serum of two rats treated with hATf (R1 + hATf and R2 + hATf). Samples were obtained from undisturbed animals (Pre), 60 min after ischemia onset and before reducing TSAT (AI), or right after the administration of hATf (AA). **(B)** Effect of i.v. hATf administration (200 mg/Kg) on the % TSAT (rat + human), calculated as explained in methods (n = 7–8 per group; *t*-test: ***p < 0.0001). **(C)** Representative TTC-stained brain slices of rats exposed to pMCAO (ligature) and treated with Veh or hATf 1 h later; slices were obtained 24 h later; scale bar, 1 cm. Effect of hATf-Low TSAT on **(D)** the infarct volume produced by pMCAO at 24 h (n = 8 per group; *t*-test: *p = 0.0181) and **(E)** the neurological score (n = 8 per group; *t*-test: *p = 0.0354). Significant positive correlations between TSAT measured after the administration of hATf and **(F)** the infarct size and **(G)** the neuroscore, both measured 24 h after pMCAO. **(H)** Effect of Low TSAT on body weight loss 24 h after pMCAO (n = 8 per group; *t*-test: *p = 0.0251).

medium increased the cytosolic Fe^{2+} levels as assessed with the turn-on Fe^{2+} specific probe Rhonox-1 (Fig. 8D). This ferrous iron (Fe^{2+}) is known to be quickly oxidized to ferric iron (Fe^{3+}) by hydrogen peroxide, producing hydroxyl radicals that have very high rate constants for the reaction with cellular molecules (e.g. ROS attack unsaturated acyl groups leading to formation of the reactive lipid-derived by-product 4-HNE, which forms adducts with several proteins that affect their function). We found that neurons treated with NMDA in the presence of
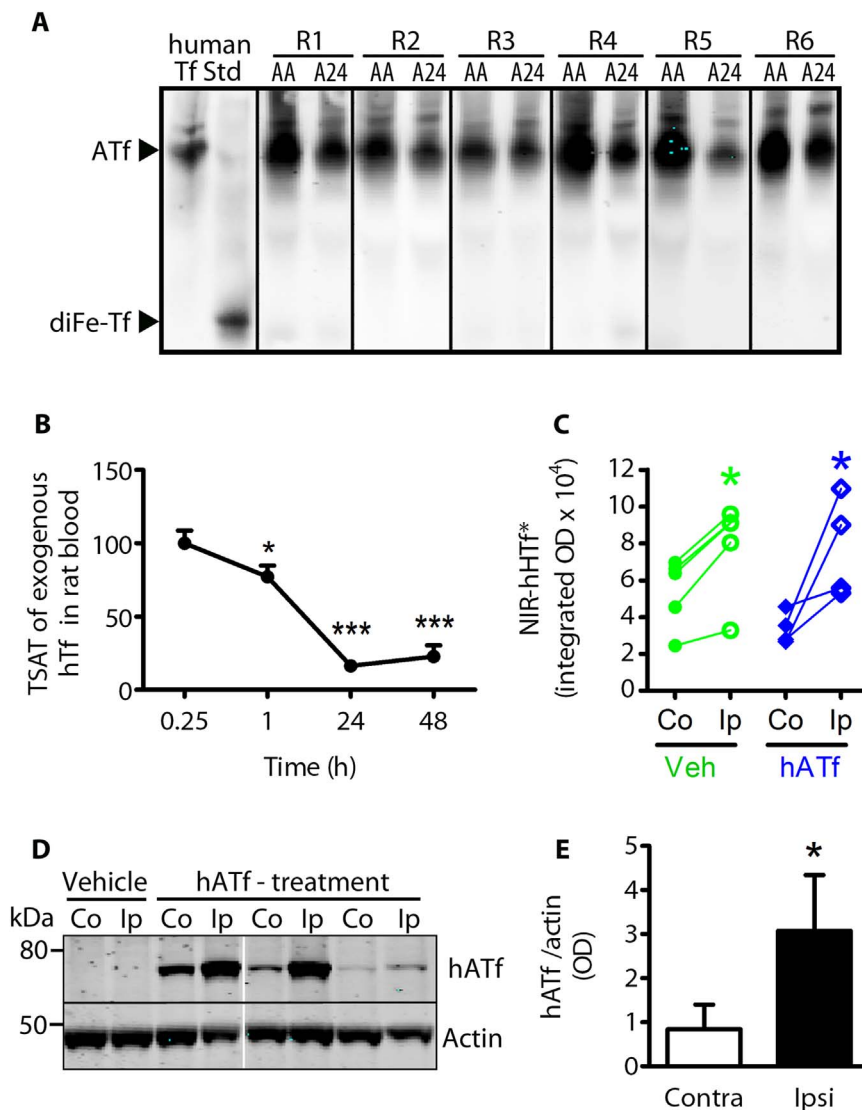
Fig. 7. Neither ATf iron-binding capacity nor a blockade of Tf extravasation explain protection by ATf. **(A)** Representative U-PAGE/WB images of the human Tf forms present in MCAO rat serum samples (R1 to R6) obtained right after the administration of hATf (AA) and 24 h later (A24). **(B)** Human HTf was administered i.v. to rats and TSAT of human Tf was determined in rat blood at different time-points. Human HTf retains most of its iron within the first hour after being administered, but loses most of the iron 24 h later (n = 4–5 per group; repeated measures one-way ANOVA: p = 0.0002, and SNK test, *p < 0.05, ***p < 0.001). **(C)** Quantification of NIR fluorescence in brains of rats exposed to tMCAO and administered NIR-hHTf* (0.8 mg/Kg) plus either Veh (green) or hATf (300 mg/Kg) (blue) at reperfusion onset. One hour later, brains were obtained and NIR fluorescence measured in the contralateral (Co) and the ipsilateral (Ip) hemispheres (n = 4–5 per group; paired *t*-test: *p = 0.0239 and **p = 0.0050 vs respective Co). **(D)** After NIR imaging, brains in (C) were processed and representative WB shows bands corresponding to exogenous hATf and actin, in Co and Ip hemispheres of Veh and hATf-treated rats 1 h after reperfusion. **(E)** Quantification of hATf levels in WB of brain hemispheres (n = 4–5 per group; paired *t*-test: *p = 0.0500).

0.065 µM hHTf generate 4-HNE (Fig. 8E), and that this effect was prevented by hATf. Also, we found a strong neuroprotective, concentration-dependent, effect of hATf on NMDA-induced neuronal death at 4 h (Fig. 8F) and a 40% reduction of the NMDA-induced neuronal death 24 h later (Fig. 8G).

Moreover, blockade of the HTf uptake with anti-TfR antibody OX26 (Fig. 9A–B), removal of the Tf present in the extracellular medium (see Fig. 9C), and the sum of Tf removal plus TfR blockade also reduced NMDA-induced neuronal death at 24 h (Fig. 9D). We also found that the well-known NMDA-induced Ca^{2+} influx turns into increased calcineurin activity, as measured through a decrease in the pDAPK1/DAPK1 ratio (Fig. 9E–F). Whereas blockade of NMDAR with MK-801 restored pDAPK1/DAPK1 to control levels, hATf had no effect on this specific parameter. None of the treatments affected DAPK1 levels as no changes were observed in DAPK1/actin ratios.

4. Discussion

Previous studies that associate iron overload conditions with increased brain damage in stroke [6,8,41] have seldom addressed the role of the iron transport protein transferrin or the role of TSAT.

The present study reveals a prompt accumulation of circulating labeled NIR-hHTf* and endogenous rat Tf into the brain areas affected by the MCAO as early as 1 h after reperfusion onset, gaining extent at 2 h.

In addition, we demonstrate that HTf enhances ROS production and OGD-induced neuronal death in vitro, even more effectively than free iron. The finding that Fe^{3+} was more efficient than Fe^{2+} in provoking neuronal death after ischemia might be attributable to the fact that Fe^{2+} has to be previously converted to Fe^{3+} to bind Tf present in our B27-supplemented medium. All the above suggests that extracellular free iron binds Tf (as shown in Fig. 2C) to be incorporated into neurons through TfR and to become deleterious in OGD conditions. OGD itself does not change neuronal TfR levels but doubles DMT-1 levels in neurons. Ischemia/excitotoxicity has been reported to increase endocytosis [42]. In such an increased Tf-TfR endocytosis scenario, more iron-loaded transferrin would gain access to endosomes and more iron would be released into the acidic endosomal lumen. Thus, increased DMT-1 transporter levels in the endosomal wall would promote increased iron egress from endosomes into neuronal cytosol.

The stroke-induced HTf extravasation to the brain parenchyma, together with the damaging effect of HTf on OGD-exposed neurons, suggests that high TSAT in blood could play a pivotal role in increasing the damage in stroke. To directly evaluate this issue, we administered HTf iv to increase TSAT to 64% (High TSAT) and found exacerbated brain damage in tMCAO rats (filament thread model; DWI in MRI time-course experiments). Conversely, administration of ATf iv to reduce TSAT at the onset of reperfusion (17–25%, Low TSAT) reduced the infarct volume in the two transient stroke models tested. Importantly,
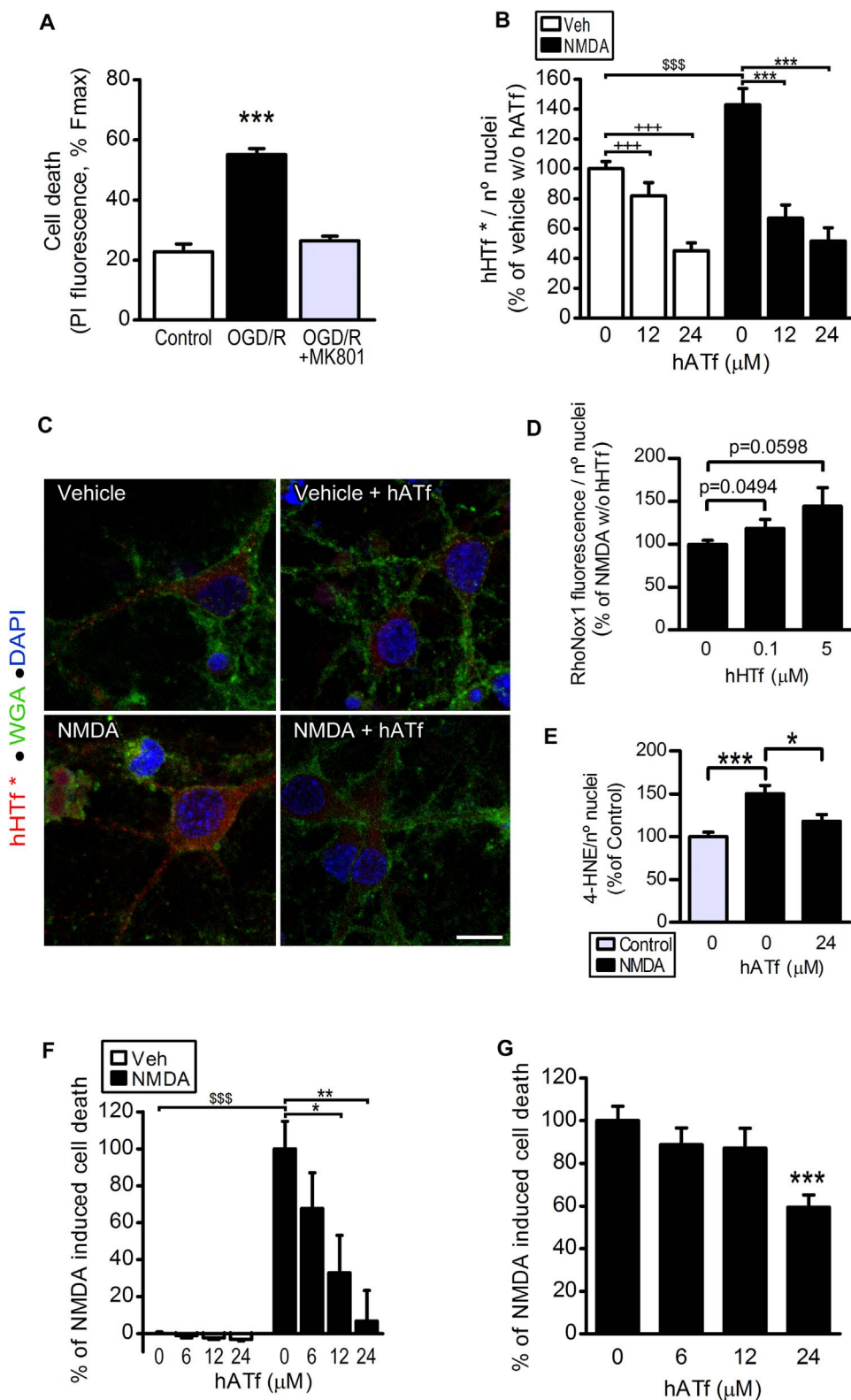
Fig. 8. Human ATf prevents NMDA-induced hHTf uptake by neurons and protects from NMDA-induced neuronal death. **(A)** MK-801 (10 μM) added at reperfusion abolished OGD-induced neuronal death in vitro observed 24 h later (5 independent experiments, ≥ 3 wells/group/experiment; *t*-test: ***p < 0.0001 vs control). **(B)** Effect of hATf on neuronal uptake of hHTf* (0.06 μM) in neuron cultures treated with NMDA (50 μM) or vehicle (3 independent experiments, ≥ 3 wells/group/experiment, 5–6 fields/well; *t*-test: $$$ p < 0.0001; one-way ANOVA: p < 0.0001 in both NMDA-treated and vehicle-treated, and SNK test: + + + and ***p < 0.001). **(C)** Representative confocal images of neurons 15 min after being treated with NMDA or Vehicle in the presence or absence of hATf (24 μM). Neurons were incubated in the presence of both hHTf* (red) and membrane-staining fluorescent WGA (green); nuclei are shown in blue; scale bar, 10 μm. **(D)** Effect of hHTf on the fluorescence turn-on of the Fe^{2+} specific fluorescent probe Rhonox-1 in neurons exposed to NMDA (50 μM) (5 independent experiments, ≥ 3 wells/group/experiment, 5–6 fields/well; *t*-test: p are indicated in the graph). **(E)** Effect of hATf on 50 μM NMDA-induced 4-HNE production (3 independent experiments, ≥ 3 wells/group/experiment, 5–6 fields/well; *t*-test: ***p < 0.0001, * p = 0.0137). **(F-G)** Effect of hATf on neuronal death in neurons exposed to NMDA (50 μM) for **(F)** 4 or **(G)** 24 h (3 independent experiments, ≥ 3 wells/group/experiment; *t*-test: $$$ p = 0.0010; one-way ANOVA: p = 0.0040, and SNK test: *p < 0.05, **p < 0.01, ***p < 0.001 vs NMDA-0 μM hATf).

serum Tf levels we measured in the experimentally-induced High and Low TSAT rats doubled those of normal rats (8.67 ± 0.89, 8.61 ± 0.57 and 4.10 ± 0.27 mg/ml, respectively), this proving that serum Tf saturation with iron, rather than Tf levels, determines the growth and extent of stroke damage. This conclusion would not be in line with the role of blood Tf levels in neuroprotection during stroke suggested by Altamura and col. [43]; their assumption was based on a significant

negative correlation of the National Institutes of Health Stroke Scale (NIHSS) score at admission and serum Tf levels in samples obtained within the next 48 h. However, NIHSS score at admission evaluates transient loss of function and not the final extent of stroke damage or neurological outcome; also, the TSAT was not determined in that study (Fig. 10).

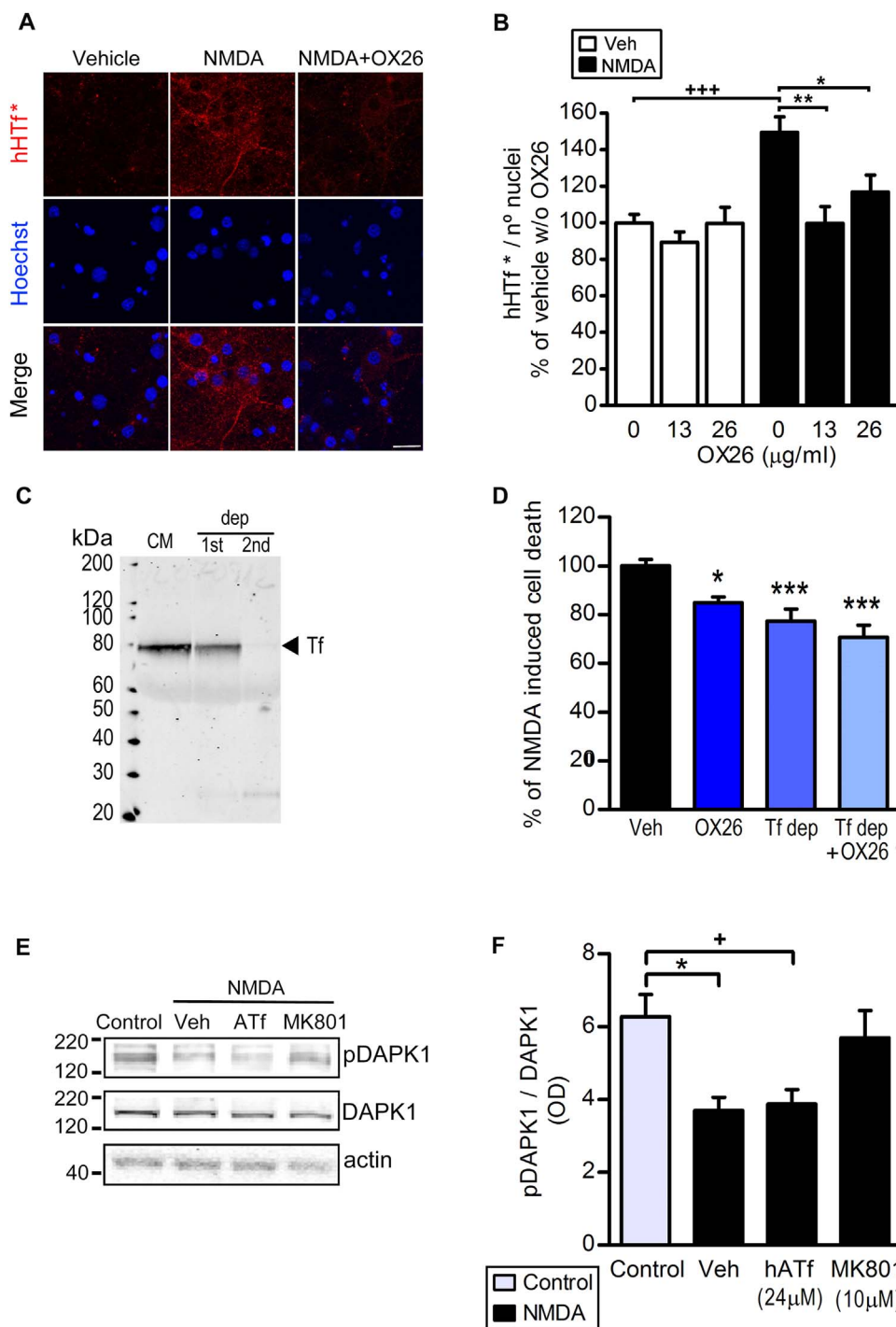The DWI-MRI experiment showed that High TSAT-induced damage

Fig. 9. Blockade of TfR and/or removal of extracellular Tf reduce NMDA-induced neuronal death. **(A)** Images show the effect of blockade of TfR (OX26) on the NMDA-induced neuronal incorporation of hHTf* (0.06 µM); scale bar, 20 µm. Neurons were treated with NMDA (50 µM). **(B)** Quantification of the effect depicted in (A) (3 independent experiments, 3 wells/group/experiment, 5 fields/well; t-test: $+++$ p < 0.0001; one-way ANOVA: p = 0.0021, and SNK test: * p < 0.05, ** p < 0.01). **(C)** SDS-PAGE/WB shows Tf depletion (dep) from conditioned medium (CM) after two (1st and 2nd) consecutive rounds of immunoprecipitation. **(D)** Blockade of TfR (OX26), incubation in Tf depleted medium (Tf dep) or both reduce NMDA-induced neuronal death at 24 h (3 independent experiments, ≥ 3 wells/group/experiment, t-test, *p = 0.0152, ***p < 0.0001). **(E)** Representative WB showing pDAPK1, DAPK1 and actin bands obtained from neurons exposed for 40 min to the treatments indicated, and **(F)** quantification of pDAK1/DAPK1 ratio from WB as in **(E)** (3 independent experiments, ≥ 3 wells/group/experiment; t-test: * p = 0.0114 and + p = 0.0169).

begins before reperfusion onset, and suggests that TfR-mediated brain uptake of transferrin molecules occurs during occlusion as reported previously for TfR-specific antibodies in conditions of severe blood flow reduction [44]. Consistent with this, we found that a reduction of TSAT from the baseline (44%) to 22% 1 h after the onset of pMCAO limited the infarct size (65% protection), the weight loss, and the neurological deficit 24 h later in this model. Also, TSAT measured right after ATf administration correlated with the 24-h infarct volume and with the neuroscore despite they received the treatment 1 h after stroke onset and did not recanalize afterwards. Remarkably, from a translational point of view, our results might be clinically relevant considering the relative large individual differences in the TSAT we determined in 33 stroke patients at admission; such differences have also been observed

in non-stroke human cohorts [10–12]. To our knowledge, there is only one (epidemiological) report, the NHANES I study, addressing a similar issue and from a different point of view. This report used retrospective TSAT determinations (made even years before the stroke event) estimated by an indirect method (serum iron/total iron-binding capacity). The authors said they found an inconsistent U-shaped association between TSAT and stroke death only in Caucasian women [45].

Since the endogenous iron-binding capacity of blood Tf exceeds by far the physiological needs, it is unlikely that exogenous hATf administered might exert protection by means of a classical chelation effect in serum (binding, sequestering and excretion of iron, as done by classical chelators such as deferoxamine). This was actually proved by the fact that exogenous hATf administered to rats does not generate
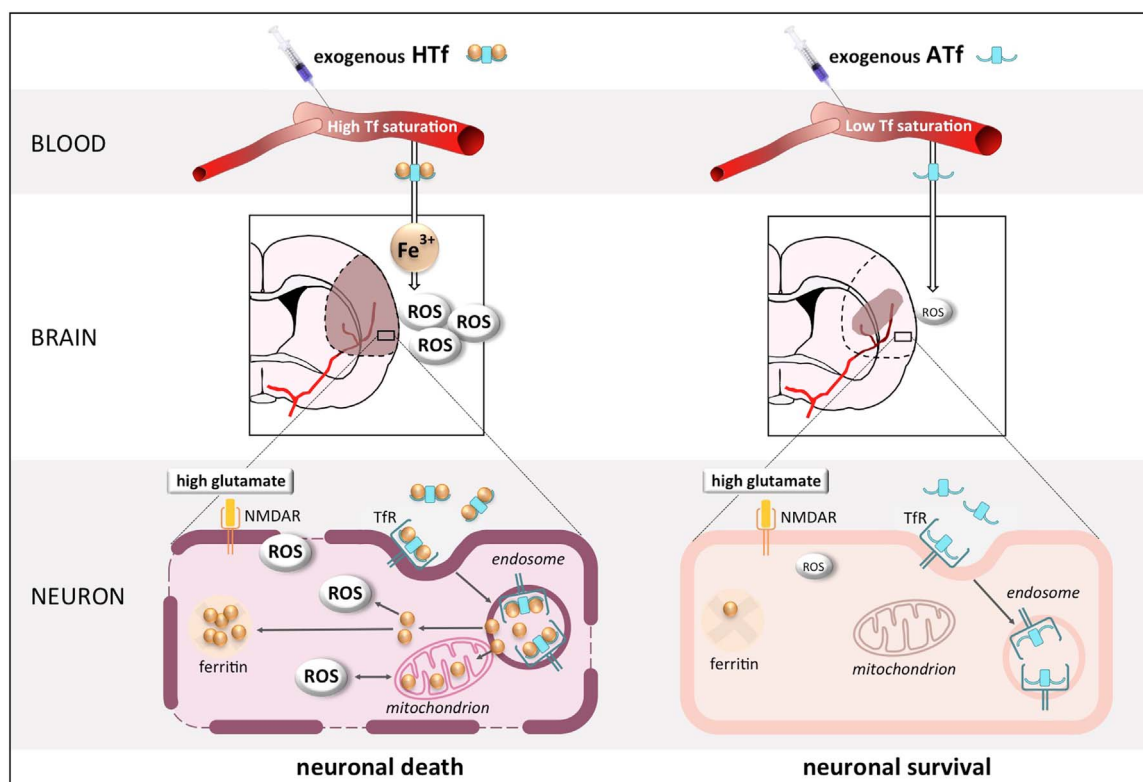
Fig. 10. Schematic representation showing that holotransferrin promotes and apotransferrin prevents a form of oxidative, iron- and NMDAR-dependent neuronal death in experimental stroke. The diagram highlights the key role of blood TSAT on neuronal fate in brain ischemic tissue in rat models of stroke, as increasing TSAT with HTf results detrimental whereas decreasing TSAT with ATf is therapeutic.

iron-bound species of human Tf in rat serum either at 1 h (not shown) or 24 h later. The therapeutic efficacy of the administration of ATf (Low TSAT) we report here was not observed in a previous report in which authors used a lower ATf dose in a model of global ischemia by circulatory arrest in pigs, and in which TSAT was not determined [46]. However, a circulatory arrest, in contrast with focal stroke models we have used, produces global brain ischemia. In addition, the iron condition of pigs in Heikkinen et al's report is unknown and in heavy iron-overload conditions apotransferrin might eventually bind iron, thus losing its protective potential.

However, in patients exposed to myeloablative conditions, Sahlstedt and col. showed that, even in extremely high blood iron overload (myeloablation results in a TSAT between 87–94%, close to full occupation of transferrin iron sites and having additional free iron in blood), the administration of a dose of ATf half the lowest we used in our report induced a significant reduction of TSAT: a single ATf administration decreased TSAT from 91% down to 30–49% 2 h later, and half the patients still showed reduced TSAT (60%) 12 h after the treatment [47]. Therefore, in the expected conditions of stroke patients at admission, 1/ using an ATf dose higher than that used by Sahlstedt, and 2/ with the stroke patients, even those suffering hemochromatosis, facing a less severe iron overload as compared to patients in Sahlstedt's report, we could expect a significant effect of the ATf treatment reducing TSAT. Therefore, since the first hours following the stroke event onset are known to be crucial to determine the stroke infarct development and the final outcome, our ATf treatment approach might represent an effective therapeutic opportunity for stroke patients given the safety record of ATf in humans [47].

With regard to the physiological mechanism involved in neuroprotection by ATf, our results in vivo indicate that protection by ATf is not related to a blockade in the extravasation of HTf. However, in neurons cultured in medium containing Tf at the saturation and concentration within the range of cerebrospinal fluid Tf [48–50], ATf completely

prevented both the NMDA-induced HTf uptake and the early NMDA-induced neuronal death (Fig. 8). The concentrations of ATf required to prevent NMDA-induced neurodegeneration fit with a competitive effect at the level of TfR, according to the reported affinity of HTf and ATf for its common receptor [18].

Ischemic-reperfused neurons are known to be exposed to NMDAR-mediated oxidative stress. In our hands, in accordance with the report by Lim and col. [51], OGD increased the lipid peroxidation product 4-HNE early after reperfusion [52]. In addition, we report here that an activation of NMDAR, known to mediate OGD-induced cell death, produces: 1/ NMDA induced HTf uptake, 2/ an increase of the cytosolic pool of labile Fe^{2+} as assessed by measuring Rhonox-1 fluorescence in the presence of added 0.1 μM hHTf, and 3/ an excess of lipid-derived product 4-HNE induced by NMDA in neurons on medium containing 0.065 μM HTf that was prevented in the presence of competing concentrations of ATf. Thus, the NMDA-induced neuronal uptake of iron loaded-transferrin increases neuronal ROS production and neuronal death. Conversely, blockade of transferrin receptors or removal of extracellular transferrin reduced cell death initiated by NMDAR overactivation to an extent similar to that exerted by ATf; this indicates the pivotal role of HTf and TfRs in mediating, at least partially, ischemic cell death. The dual involvement of excess ROS/lipid peroxidation and the requirement of transferrin-TfR-mediated iron uptake we observed in the present study has also been reported as key features in some ferroptosis models [53,54], thus suggesting that at least part of the ischemic neurons may degenerate undergoing a form of ferroptosis. The study of this possibility goes beyond the objective of the present work but deserves attention, especially considering the protective role of apotransferrin in experimental ischemic stroke.

The classical transferrin-TfR-mediated endocytosis model [14,55] describes that HTf-TfR is internalized in endosomes, and establishes that, whereas endosome free iron is released into cytosol, ATf is not; instead the endosomal ATf-TfR complex returns to the cell membrane.

Also, the presence of some ATf molecules in the cytosol of ischemic neurons that might bind residual intracellular free iron is unlikely and has not been supported by experimental evidence to date; this role (cytosolic free iron binding) is assumed by the molecule ferritin.

It is well known that following NMDAR activation, Ca^{2+} influx increases the activity of neuronal calcineurin which, in turn, dephosphorylates its downstream target DAPK1 [56]. Also, our results show that ATf, that reduced the Tf/TfR-mediated ROS-4-HNE production pathway but did not affect the Ca2 +-mediated DAPK1 signaling pathway, was able to reduce neuronal death. Therefore, our results indicate that these two pathways initiated by NMDAR overactivation contribute, in an additive mode, to neuronal death and that ATf is able to reduce neuronal death without targeting NMDA receptor canonical signaling.

In summary, we show that holotransferrin promotes and apotransferrin prevents a form of oxidative, iron- and NMDAR-initiated neuronal death in experimental stroke. Our results highlight the key role of blood TSAT on infarct size and neurological outcome in rat models of stroke, as increasing TSAT with HTf results detrimental whereas decreasing TSAT with ATf is therapeutic.

Acknowledgments

Author contributions

T.G., N.D.-R and O.M.-S. formulated the hypothesis and organized the study. I.L., J.C., M.M. and A.D. contributed to the experimental design and M.M. and A.D. recruited and provided samples from the TANDEM-1 cohort. N.D.-R., O.M.-S., T.G. and V.G. designed, performed and analyzed in vitro studies. N.D.-R., O.M.-S. and I.G.-Y. designed, conducted and analyzed the experiments in vivo using experimental ligature stroke models. J.B.S., E.A. and M.C.-R. designed, conducted and analysed the intraluminal non-MRI MCAO experiments. P.R.-C. and J.V. conducted and analysed the MRI studies of the MCAO experiment. N.D.-R., T.G. and O.M.-S. wrote the manuscript.

References

[1] H. Chen, H. Yoshioka, G.S. Kim, J.E. Jung, N. Okami, H. Sakata, C.M. Maier, P. Narasimhan, C.E. Goeders, P.H. Chan, Oxidative stress in ischemic brain damage: mechanisms of cell death and potential molecular targets for neuroprotection, Antioxid. Redox Signal. 14 (2011) 1505–1517, http://dx.doi.org/10.1089/ars.2010.3576.

[2] D.B. Kell, Iron behaving badly: inappropriate iron chelation as a major contributor to the aetiology of vascular and other progressive inflammatory and degenerative diseases, BMC Med. Genom. 2 (2009) 2, http://dx.doi.org/10.1186/1755-8794-2-2.

[3] A. Dávalos, J.M. Fernandez-Real, W. Ricart, S. Soler, A. Molins, E. Planas, D. Genis, Iron-related damage in acute ischemic stroke, Stroke 25 (1994) 1543–1546.

[4] M. Castellanos, N. Puig, T. Carbonell, J. Castillo, J.M. Martinez, R. Rama, A. Dávalos, Iron intake increases infarct volume after permanent middle cerebral artery occlusion in rats, Brain Res. 952 (2002) 1–6, http://dx.doi.org/10.1016/S0006-8993(02)03179-7.

[5] A. Gamez, T. Carbonell, R. Rama, Does nitric oxide contribute to iron-dependent brain injury after experimental cerebral ischaemia? J. Physiol. Biochem. 59 (2003) 249–254.

[6] S.H. Mehta, R.C. Webb, A. Ergul, A. Tawfik, A.M. Dorrance, Neuroprotection by tempol in a model of iron-induced oxidative stress in acute ischemic stroke, Am. J. Physiol. Regul. Integr. Comp. Physiol. 286 (2004) R283–R288, http://dx.doi.org/10.1152/ajpregu.00446.2002.

[7] M. Millan, T. Sobrino, M. Castellanos, F. Nombela, J.F. Arenillas, E. Riva, I. Cristobo, M.M. Garcia, J. Vivancos, J. Serena, M.A. Moro, J. Castillo, A. Davalos, Increased body iron stores are associated with poor outcome after thrombolytic treatment in acute stroke, Stroke 38 (2007) 90–95, http://dx.doi.org/10.1161/01.STR.0000251798.25803.e0.

[8] I. García-Yébenes, M. Sobrado, A. Moraga, J.G. Zarruk, V.G. Romera, J.M. Pradillo, N. Perez De La Ossa, M.A. Moro, A. Dávalos, I. Lizasoain, Iron overload, measured as serum ferritin, increases brain damage induced by focal ischemia and early reperfusion, Neurochem. Int. 61 (2012) 1364–1369, http://dx.doi.org/10.1016/j.neuint.2012.09.014.

[9] E. Millerot, A.S. Prigent-Tessier, N.M. Bertrand, P.J.C. Faure, C.M. Mossiat, M.E. Giroud, A.G. Beley, C. Marie, Serum ferritin in stroke: a marker of increased body iron stores or stroke severity? J. Cereb. Blood Flow. Metab. 25 (2005) 1386–1393, http://dx.doi.org/10.1038/sj.jcbfm.9600140.

[10] P.C. Adams, D.M. Reboussin, J.C. Barton, C.E. McLaren, J.H. Eckfeldt, G.D. McLaren, F.W. Dawkins, R.T. Acton, E.L. Harris, V.R. Gordeuk, C. Leiendecker-Foster, M. Speechley, B.M. Snively, J.L. Holup, E. Thomson, P. Sholinsky, Hemochromatosis and iron-overload screening in a racially diverse population, N. Engl. J. Med. 352 (2005) 1769–1778, http://dx.doi.org/10.1056/NEJMoa041534.

[11] B. De Valk, M.A. Addicks, I. Gosriwatana, S. Lu, R.C. Hider, J.J.M. Marx, Non-transferrin-bound iron is present in serum of hereditary haemochromatosis heterozygotes, Eur. J. Clin. Investig. 30 (2000) 248–251, http://dx.doi.org/10.1046/j.1365-2362.2000.00628.x.

[12] B.A.C. Van Dijk, C.M.M. Laarakkers, S.M. Klaver, E.M.G. Jacobs, L.J.H. Van Tits, M.C.H. Janssen, D.W. Swinkels, Serum hepcidin levels are innately low in HFE-related haemochromatosis but differ between C282Y-homozygotes with elevated and normal ferritin levels, Br. J. Haematol. 142 (2008) 979–985, http://dx.doi.org/10.1111/j.1365-2141.2008.07273.x.

[13] J.A. Gaasch, P.R. Lockman, W.J. Geldenhuys, D.D. Allen, C.J. Van Der Schyf, Brain iron toxicity: differential responses of astrocytes, neurons, and endothelial cells, Neurochem. Res. 32 (2007) 1196–1208, http://dx.doi.org/10.1007/s11064-007-9290-4.

[14] A.N. Luck, A.B. Mason, Transferrin-mediated cellular iron delivery, Curr. Top. Membr. 69 (2012) 3–35, http://dx.doi.org/10.1016/B978-0-12-394390-3.00001-X.

[15] L. Descamps, M.P. Dehouck, G. Torpier, R. Cecchelli, Receptor-mediated transcytosis of transferrin through blood-brain barrier endothelial cells, Am. J. Physiol. 270 (1996) H1149–H1158.

[16] J.B. Fishman, J.B. Rubin, J.V. Handrahan, J.R. Connor, R.E. Fine, Receptor-mediated transcytosis of transferrin across the blood-brain barrier, J. Neurosci. Res. 18 (1987) 299–304, http://dx.doi.org/10.1002/jnr.490180206.

[17] Y.J. Yu, J.K. Atwal, Y. Zhang, R.K. Tong, K.R. Wildsmith, C. Tan, N. Bien-Ly, M. Hersom, J.A. Maloney, W.J. Meilandt, D. Bumbaca, K. Gadkar, K. Hoyte, W. Luk, Y. Lu, J.A. Ernst, K. Scearce-Levie, J.A. Couch, M.S. Dennis, R.J. Watts, Therapeutic bispecific antibodies cross the blood-brain barrier in nonhuman primates, Sci. Transl. Med. 6 (2014) 261ra154, http://dx.doi.org/10.1126/scitranslmed.3009835.

[18] A. Mason, Q. He, B. Tam, R. MacGillivray, R. Woodworth, Mutagenesis of the aspartic acid ligands in human serum transferrin: lobe-lobe interaction and conformation as revealed by antibody, receptor-binding and iron-release studies, Biochem. J. 330 (1998) 35–40.

[19] S.P. Young, A. Bomford, R. Williams, The effect of the iron saturation of transferrin on its binding and uptake by rabbit reticulocytes, Biochem. J. 219 (1984) 505–510, http://dx.doi.org/10.1042/bj2190505.

[20] J.H. Cheah, S.F. Kim, L.D. Hester, K.W. Clancy, S.E. Patterson, V. Papadopoulos, S.H. Snyder, NMDA receptor-nitric oxide transmission mediates neuronal iron homeostasis via the GTPase Dexras1, Neuron 51 (2006) 431–440, http://dx.doi.org/10.1016/j.neuron.2006.07.011.

[21] P. Yu, M. Zhang, H. Ding, X. Di, P. Guan, S. Wang, Z. Shi, D. Jiang, X. Duan, Effect of glutamate on brain iron metabolism and the regulation mechanism, J. Drug Metab. Toxicol. 6 (2015) 190, http://dx.doi.org/10.4172/2157-7609.1000190.

[22] S.T. Chen, C.Y. Hsu, E.L. Hogan, H. Maricq, J.D. Balentine, A model of focal ischemic stroke in the rat: reproducible extensive cortical infarction, Stroke 17 (1986) 738–743, http://dx.doi.org/10.1161/01.STR.17.4.738.

[23] E.Z. Longa, P.R. Weinstein, S. Carlson, R. Cummins, Reversible middle cerebral artery occlusion without craniectomy in rats, Stroke 20 (1989) 84–91, http://dx.doi.org/10.1161/01.STR.20.1.84.

[24] J.B. Salom, F.J. Pérez-Asensio, M.C. Burguete, N. Marín, C. Pitarch, G. Torregrosa, F.J. Romero, E. Alborch, Single-dose ebselen does not afford sustained neuroprotection to rats subjected to severe focal cerebral ischemia, Eur. J. Pharmacol. 495 (2004) 55–62, http://dx.doi.org/10.1016/j.ejphar.2004.05.024.

[25] C. Orset, R. Macrez, A.R. Young, D. Vivien, Mouse model of in situ thromboembolic stroke and reperfusion, Stroke 38 (2007) 2771–2778, http://dx.doi.org/10.1007/978-1-4939-5620-3_6.

[26] K. Türeyen, R. Vemuganti, K.A. Sailor, R.J. Dempsey, Infarct volume quantification in mouse focal cerebral ischemia: a comparison of triphenyltetrazolium chloride and cresyl violet staining techniques, J. Neurosci. Methods 139 (2004) 203–207, http://dx.doi.org/10.1016/j.jneumeth.2004.04.029.

[27] S.L. Byrne, A.B. Mason, Human serum transferrin: a tale of two lobes. Urea gel and steady state fluorescence analysis of recombinant transferrins as a function of pH,

time, and the soluble portion of the transferrin receptor, J. Biol. Inorg. Chem. 14 (2009) 771–781, http://dx.doi.org/10.1007/s00775-009-0491-y.Human.

[28] M.H. Nagaoka, T. Maitani, Diffeered preferential iron-binding lobe in human transferrin depending on the presence of bicarbonate detected by HPLC / high-resolution inductively coupled plasma mass spectrometry, Biochim. Biophys. Acta 1523 (2000) 182–188.

[29] B. Scheiber-Mojdehkar, Non-transferrin-bound iron in the serum of hemodialysis patients who receive ferric saccharate: no correlation to peroxide generation, J. Am. Soc. Nephrol. 15 (2004) 1648–1655, http://dx.doi.org/10.1097/01.ASN.0000130149.18412.56.

[30] D.G. Makey, U.S. Seal, The detection of four molecular forms of human transferrin during the iron binding process, Biochim. Biophys. Acta 453 (1976) 250–256, http://dx.doi.org/10.1016/0005-2795(76)90270-1.

[31] R. Agarwal, Transferrin saturation with intravenous irons: an in vitro study, Kidney Int. 66 (2004) 1139–1144, http://dx.doi.org/10.1111/j.1523-1755.2004.00864.x.

[32] E. Kitsati, Liakos, M.D. Mantzaris, S. Vasakos, E. Kyratzopoulou, E.A. Petros Eliadis, E. Kokkolou, D.G. Georgios Sferopoulos, Avgi Mamalaki, Konstantinos Siamopoulos, Rapid elevation of transferrin saturation and serum hepcidin concentration in hemodialysis patients after intravenous iron infusion, Haematologica 100 (2015) 80–83.

[33] K. Harada, A. Kuniyasu, H. Nakayama, M. Nakayama, T. Matsunaga, Y. Uji, H. Sugiuchi, H. Okabe, Separation of human serum transferrins with different iron-binding states by high-performance liquid chromatography using a pyridinium polymer column, J. Chromatogr. B Anal. Technol. Biomed. Life Sci. 767 (2002) 45–51, http://dx.doi.org/10.1016/S0378-4347(01)00529-1.

[34] J. Ponce, D. Brea, M. Carrascal, V. Guirao, N. DeGregorio-Rocasolano, T. Sobrino, J. Castillo, A. Dávalos, T. Gasull, The effect of simvastatin on the proteome of detergent-resistant membrane domains: decreases of specific proteins previously related to cytoskeleton regulation, calcium homeostasis and cell fate, Proteomics 10 (2010) 1954–1965, http://dx.doi.org/10.1002/pmic.200900055.

[35] Y. Chen, B. Stevens, J. Chang, J. Milbrandt, B.A. Barres, J.W. Hell, NS21: re-defined and modified supplement B27 for neuronal cultures, J. Neurosci. Methods 171 (2008) 239–247, http://dx.doi.org/10.1016/j.jneumeth.2008.03.013.NS21.

[36] M. Karlsson, T. Kurz, U.T. Brunk, S.E. Nilsson, C.I. Frennesson, What does the commonly used DCF test for oxidative stress really show? Biochem. J. 428 (2010) 183–190, http://dx.doi.org/10.1042/BJ20100208.

[37] T. Hirayama, K. Okuda, H. Nagasawa, A highly selective turn-on fluorescent probe for iron(ii) to visualize labile iron in living cells, Chem. Sci. 4 (2013) 1250–1256, http://dx.doi.org/10.1039/c2sc21649c.

[38] J.G. Rudolph, J.J. Lemasters, F.T. Crews, Use of a multiwell fluorescence scanner with propidium iodide to assess NMDA mediated excitotoxicity in rat cortical neuronal cultures, Neurosci. Lett. 221 (1997) 149–152, http://dx.doi.org/10.1016/S0304-3940(96)13313-9.

[39] T. Gasull, N. Degregorio-rocasolano, R. Trullas, Overactivation of alpha-amino-3-hydroxy-5-methylisoxazole-4-propionate and N-methyl-d-aspartate but not kainate receptors inhibits phosphatidylcholine synthesis before excitotoxic neuronal death, J. Neurochem. 77 (2001) 13–22.

[40] K.A. Hossmann, Cerebral ischemia: models, methods and outcomes, Neuropharmacology 55 (2008) 257–270, http://dx.doi.org/10.1016/j.neuropharm.2007.12.004.

[41] A. Dávalos, J. Castillo, J. Marrugat, J.M. Fernandez-Real, A. Armengou, P. Cacabelos, R. Rama, Body iron stores and early neurologic deterioration in acute cerebral infarction, Neurology 54 (2000) 1568–1574.

[42] A. Vaslin, J. Puyal, T. Borsello, P.G.H. Clarke, Excitotoxicity-related endocytosis in cortical neurons, J. Neurochem. 102 (2007) 789–800, http://dx.doi.org/10.1111/j.1471-4159.2007.04564.x.

[43] C. Altamura, R. Squitti, P. Pasqualetti, C. Gaudino, P. Palazzo, F. Tibuzzi, D. Lupoi, M. Cortesi, P.M. Rossini, F. Vernieri, Ceruloplasmin/Transferrin system is related to clinical status in acute stroke, Stroke 40 (2009) 1282–1288, http://dx.doi.org/10.1161/STROKEAHA.108.536714.

[44] J. Hao, U. Bickel, Transferrin receptor mediated brain uptake during ischemia and reperfusion, J. Pharm. Pharm. Sci. 16 (2013) 541–550.

[45] R.F. Gillum, C.T. Sempos, D.M. Makuc, A.C. Looker, C.-Y. Chien, D.D. Ingram, Serum transferrin saturation, stroke incidence, and mortality in women and men. The NHANES I epidemiologic followup study, Am. J. Epidemiol. 144 (1996) 59–68, http://dx.doi.org/10.1093/oxfordjournals.aje.a008855.

[46] J. Heikkinen, J. Koskenkari, T. Kaakinen, S. Dahlbacka, K. Kiviluoma, T. Salomäki, P. Laurila, J. Hirvonen, F. Biancari, J. Parkkinen, T. Juvonen, Apotransferrin, C1-esterase inhibitor, and alpha 1-acid glycoprotein for cerebral protection during experimental hypothermic circulatory arrest, Scand. Cardiovasc. J. 38 (2004) 178–186, http://dx.doi.org/10.1080/14017430410028618.

[47] L. Sahlstedt, L. Von Bonsdorff, F. Ebeling, T. Ruutu, J. Parkkinen, Effective binding of free iron by a single intravenous dose of human apotransferrin in haematological stem cell transplant patients, Br. J. Haematol. 119 (2002) 547–553, http://dx.doi.org/10.1046/j.1365-2141.2002.03836.x.

[48] M.W. Bradbury, Transport of iron in the blood-brain-cerebrospinal fluid system, J. Neurochem. 69 (1997) 443–454, http://dx.doi.org/10.1046/j.1471-4159.1997.69020443.x.

[49] M. Khalil, R. Riedlbauer, C. Langkammer, C. Enzinger, S. Ropele, T. Stojakovic, H. Scharnagl, V. Culea, A. Petzold, C. Teunissen, J.-J. Archelos, S. Fuchs, F. Fazekas, Cerebrospinal fluid transferrin levels are reduced in patients with early multiple sclerosis, Mult. Scler. J. (2014) 1569–1577, http://dx.doi.org/10.1177/1352458514530020.

[50] T. Moos, P.S. Oates, E.H. Morgan, Iron-independent neuronal expression of transferrin receptor mRNA in the rat, Brain Res. Mol. Brain Res. 72 (1999) 231–234, http://dx.doi.org/10.1016/S0169-328X(99)00226-0.

[51] J.H. Lim, J.C. Lee, Y.H. Lee, I.Y. Choi, Y.K. Oh, H.S. Kim, J.S. Park, W.K. Kim, Simvastatin prevents oxygen and glucose deprivation/reoxygenation-induced death of cortical neurons by reducing the production and toxicity of 4-hydroxy-2E-nonenal, J. Neurochem. 97 (2006) 140–150, http://dx.doi.org/10.1111/j.1471-4159.2006.03715.x.

[52] V. Guirao, O. Martí-Sistac, N. DeGregorio-Rocasolano, J. Ponce, A. Dávalos, T. Gasull, Specific rescue by ortho-hydroxy atorvastatin of cortical GABAergic neurons from previous oxygen/glucose deprivation: role of pCREB, J. Neurochem. (2017), http://dx.doi.org/10.1111/jnc.14210.

[53] J.Y. Cao, S.J. Dixon, Mechanisms of ferroptosis, Cell. Mol. Life Sci. 73 (2016) 2195–2209, http://dx.doi.org/10.1007/s00018-016-2194-1.

[54] J.P.F. Angeli, R. Shah, D.A. Pratt, M. Conrad, Ferroptosis inhibition: mechanisms and opportunities, Trends Pharmacol. Sci. 38 (2017) 489–498, http://dx.doi.org/10.1016/j.tips.2017.02.005.

[55] I. De Domenico, D. McVey Ward, J. Kaplan, Regulation of iron acquisition and storage: consequences for iron-linked disorders, Nat. Rev. Mol. Cell Biol. 9 (2008) 72–81, http://dx.doi.org/10.1038/nrm2295.

[56] W. Tu, X. Xu, L. Peng, X. Zhong, W. Zhang, M.M. Soundarapandian, C. Balel, M. Wang, N. Jia, W. Zhang, F. Lew, S.L. Chan, Y. Chen, Y. Lu, DAPK1 Interaction with NMDA receptor NR2B subunits mediates brain damage in stroke, Cell 140 (2010) 222–234, http://dx.doi.org/10.1016/j.cell.2009.12.055.